Keynote - Nanomanufacturing & Functional Ceramics: How New Material Platforms Will Reshape Industry

Perena Gouma, Ph.D.

Edward Orton Jr., Chair in Ceramics Engineering

acrl.osu.edu

THE OHIO STATE UNIVERSITY

NANOSCALE CERAMICS AND POLYMORPH SELECTION

Bulk vs Nano-Ceramic Oxides

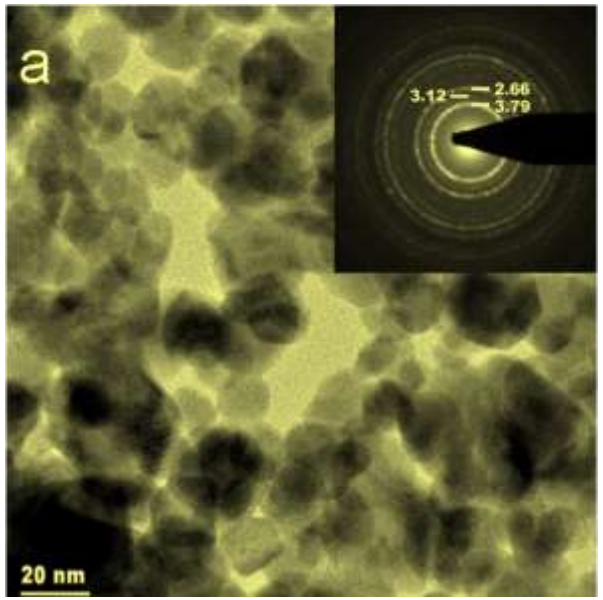
Comparison of bulk with nano phase at ambient T & P

Metal Oxide at ambient conditions	Bulk phase		Nano Phase			
	Phase	Conditions of temperature and pressure	Phase	Critical particle size	Temperature	*Ref.*
SnO_2	Rutile-type tetragonal phase	RT and 1 atm	$CaCl_2$-type orthorhombic phase	Below 50nm	RT and 1 atm	*112, 113, 114, 115*
In_2O_3	Cubic structure	RT and 1 atm	Cubic structure + Corundum-type hexagonal structure	Below 80nm	RT and 1 atm	*126, 127, 128, 129*
Al_2O_3	Corundum type trigonal α-phase	RT and 1 atm	Cubic γ phase	Below 17nm and below 473K	RT and 1 atm	*68, 46, 47*
TiO_2	Rutile	RT and 1 atm	Anatase	Below 11nm	RT and 1 atm	*38, 41*
MoO_3	Orthorhombic α phase	RT and 1 atm	Orthorhombic α + Hexagonal phase	Below 200nm and 443 to 673K	RT and 1 atm	*50, 51*
WO_3	Triclinic δ-phase	RT and 1 atm	Monoclinic ε phase	Nanosize	RT and 1 atm	*83, 57, 59*
ZrO_2	Monoclinic phase	RT and 1 atm	Tetragonal phase	Below 18nm	RT and 1 atm	*39, 142, 143*

"Polymorphism in nanocrystalline binary metal oxides", S. Sood, P. Gouma, Nanomaterials and Energy, 2(NME2), 1-15(2013). - Supplementary file

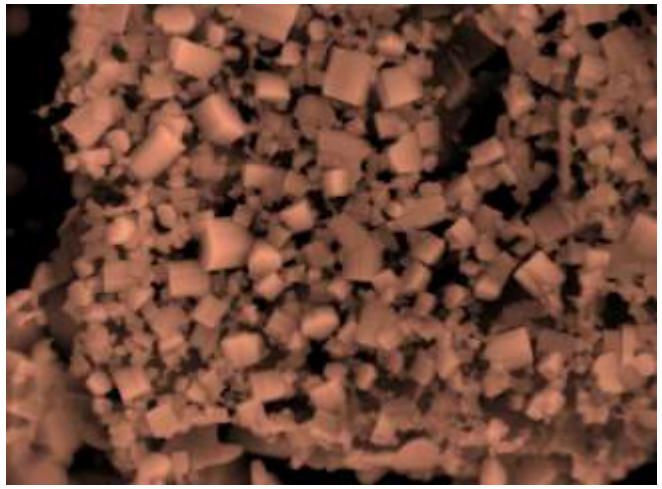
Nanoscale Processing of Metal Oxides: a “toolbox” of new phases to use as gas sensors

Combustion/ Flame spray pyrolysis



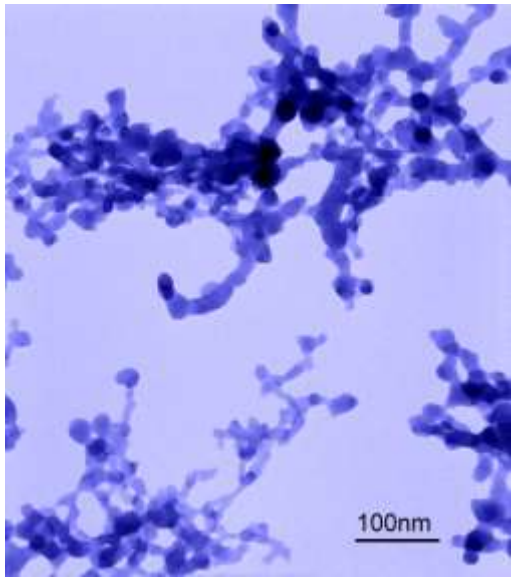
L. Wang, Ph.D. Thesis, SUNY Stony Brook, 2008

Hydrothermal process

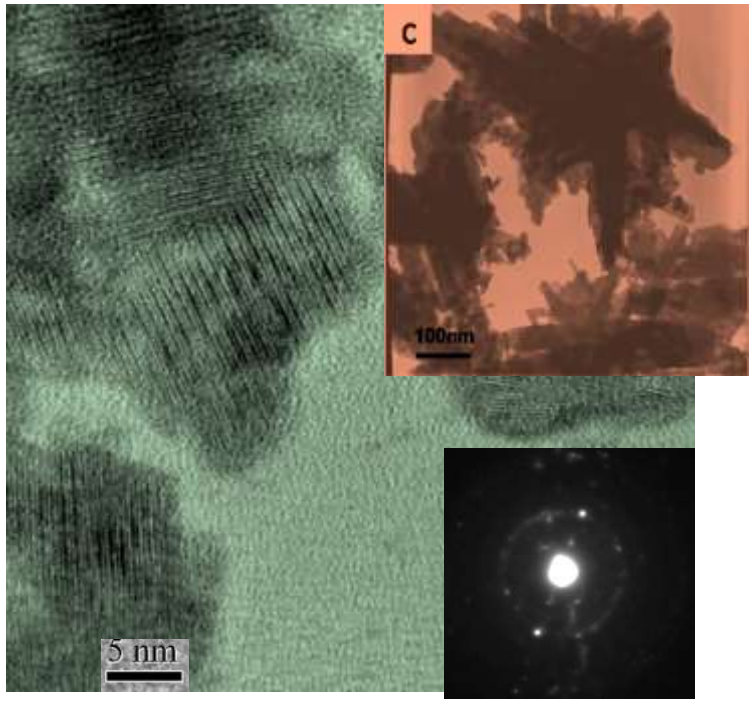


K. Kalyanasundaram, Ph.D. Thesis, SUNY Stony Brook, 2007

Sol-gel process



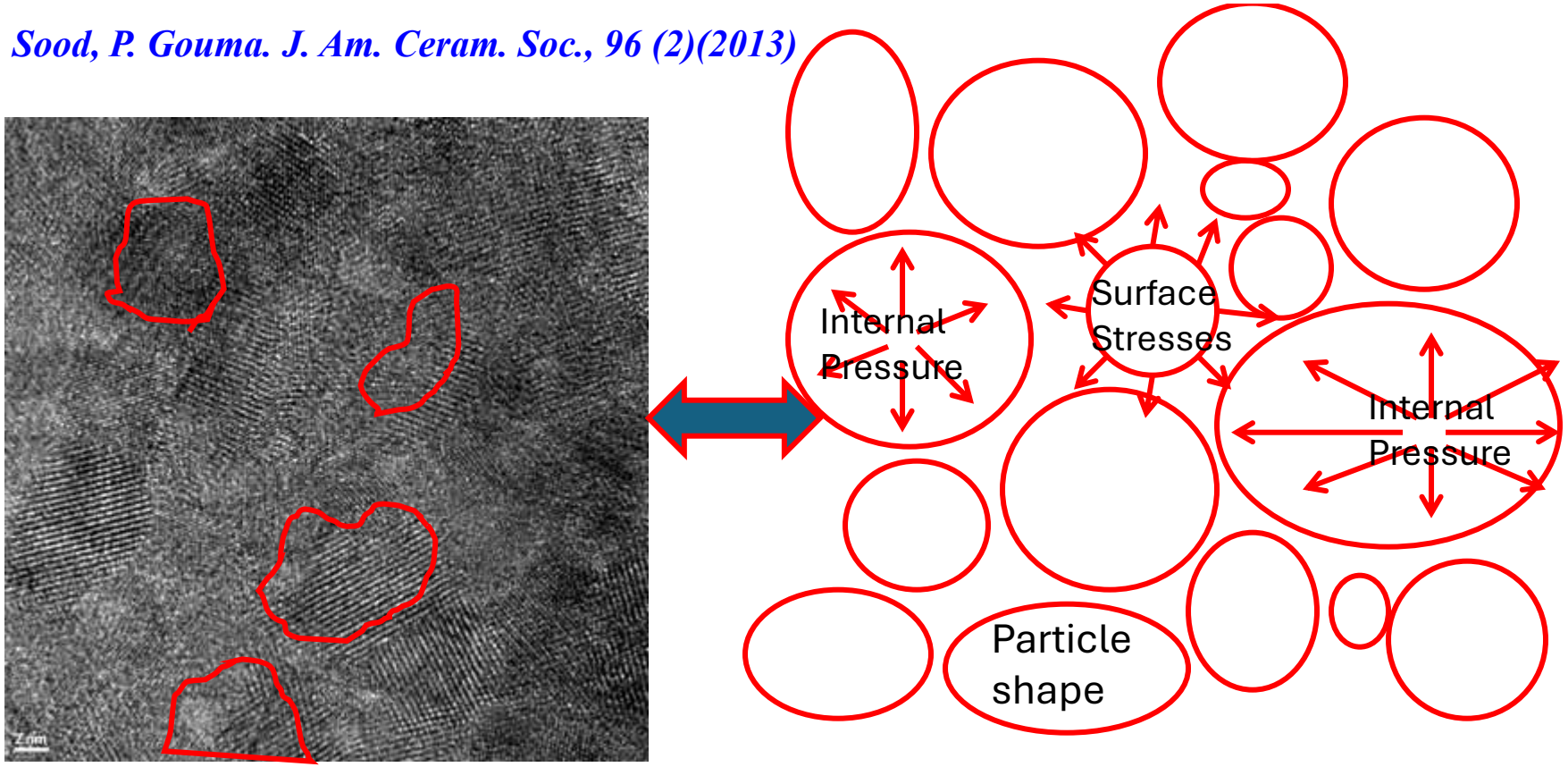
Solvothermal process



Heuristic Approach to Phase Stability

Surface effects	Internal pressure effects	Particle shape effects
$\Delta G_S^{\beta\rightarrow\alpha}(r) = (3.\gamma^{\beta}.V^{\beta}_m - 3.\gamma^{\alpha}.V^{\alpha}_m)/r$	$\Delta G_P^{\beta\rightarrow\alpha}(r) = (2.f^{\beta}_s.V^{\beta}_m - 2.f^{\alpha}_s.V^{\alpha}_m)/r$	$\Delta G_G^{\beta\rightarrow\alpha}(r) = g.(\gamma^{\alpha} - \gamma^{\beta})/N^{1/3}$ $= -\alpha.\{\Delta^{\circ}H_f^{\alpha}(T) - \Delta^{\circ}H_f^{\beta}(T)\}/2.r$

S. Sood, P. Gouma. J. Am. Ceram. Soc., 96 (2)(2013)



$$\Delta G = \Delta S.T + \Delta G_S^{\beta\rightarrow\alpha} + \Delta G_P^{\beta\rightarrow\alpha} + \Delta G_G^{\beta\rightarrow\alpha}$$

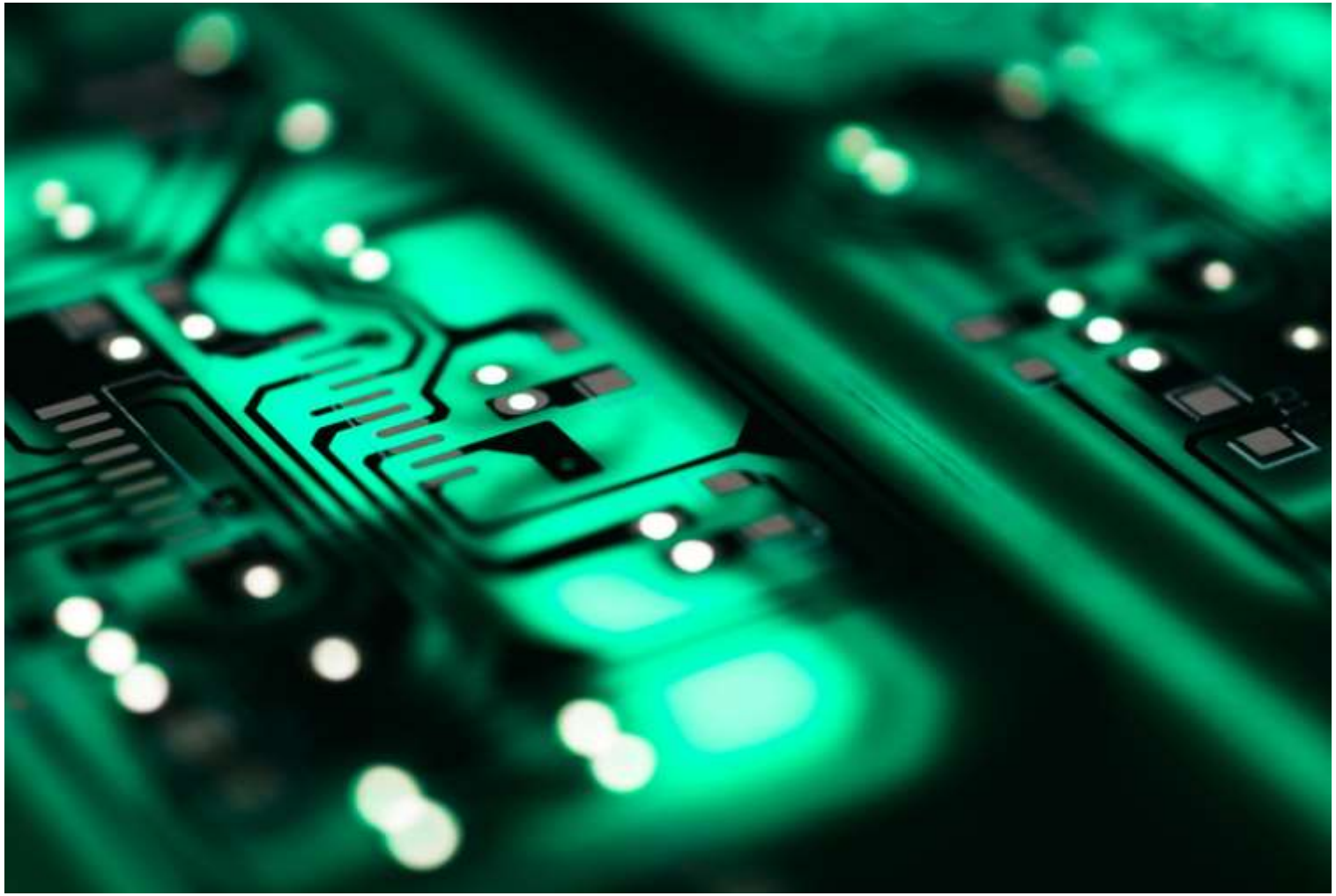
Heuristic Formula Calculates Critical Particle Size for Metastable to Stable Polymorph Transitions:

$$r_c^{\beta\rightarrow\alpha}(T) = \{M.(\gamma^{\alpha}/\rho^{\alpha} - \gamma^{\beta}/\rho^{\beta} + 2.f_s^{\beta}/\rho^{\beta} - 2.f_s^{\alpha}/\rho^{\alpha})\}$$

CASE STUDIES

Metal Oxide	$\Delta^{-}H_t(T)$	γ^{α}	ρ^{α}	γ^{γ}	ρ^{γ}	Theoretical Critical Particle size	Experimental Critical Particle size
γ-Alumina to α-Alumina	22.17 kJ/mol	2.08 J/m^2	4.00 g/cm^3	0.79 J/m^2	3.65 g/cm^3	4.0nm to 2.6nm	3.2nm at 473K
Anatase titania to rutile titania	2.61 kJ/mol	1.25 J/m^2	3.893 g/cm^3	1.84 J/m^2	4.249 g/cm^3	9.9nm to 8.5nm	8nm at 673K
Tetra Zirconia to Mono Zirconia	10±1 kJ/mol	6.4 J/m^2	5.68 g/cm^3	2.1 J/m^2	6.09 g/cm^3	28nm to 27.1nm	30nm
γ-Fe_2O_3 to α-Fe_2O_3	13.7 KJ/mol	0.71 J/m^2	5.49g/cm^3	1.9±0.3 J/m^2	5.242 g/cm^3	6.5nm to 7.9nm	About 5nm

"Polymorphic phase transitions in nanocrystalline binary metal oxides", S. Sood, P. Gouma. J. Am. Ceram. Soc., 96 [2], 351–354(2013)



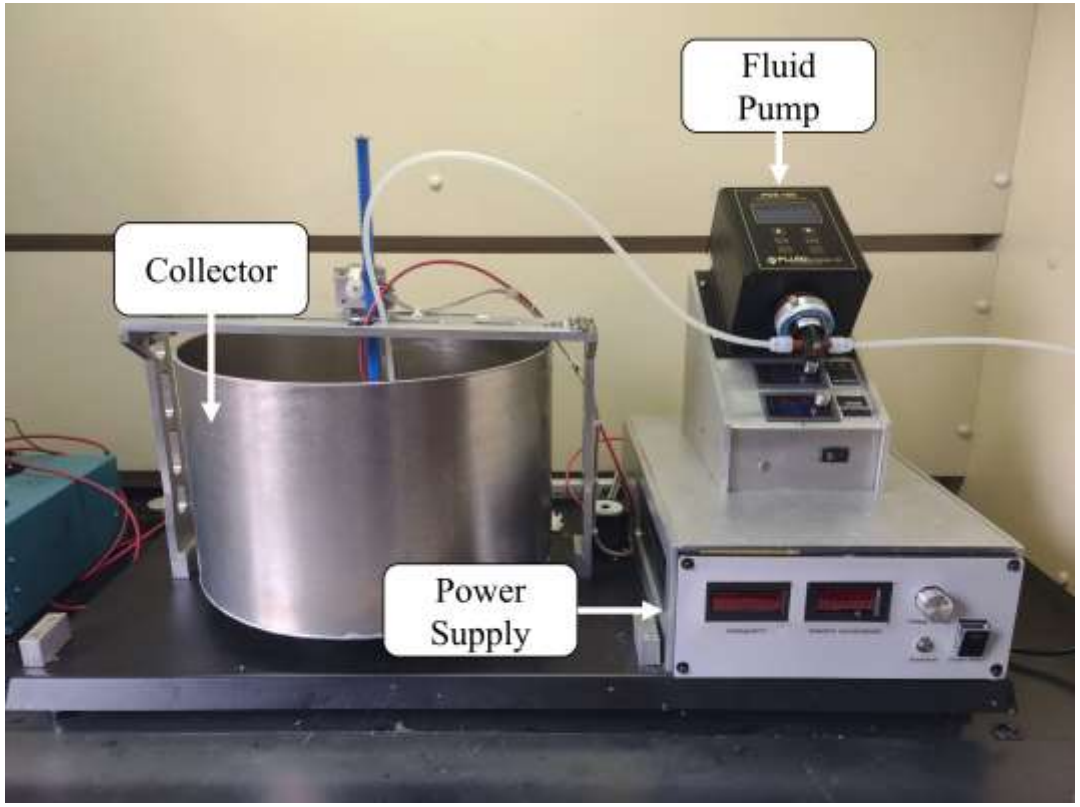
NEW ENGINEERING

Scalable Material Technologies

Flame Spray Pyrolysis



High Throughput Electrospinning

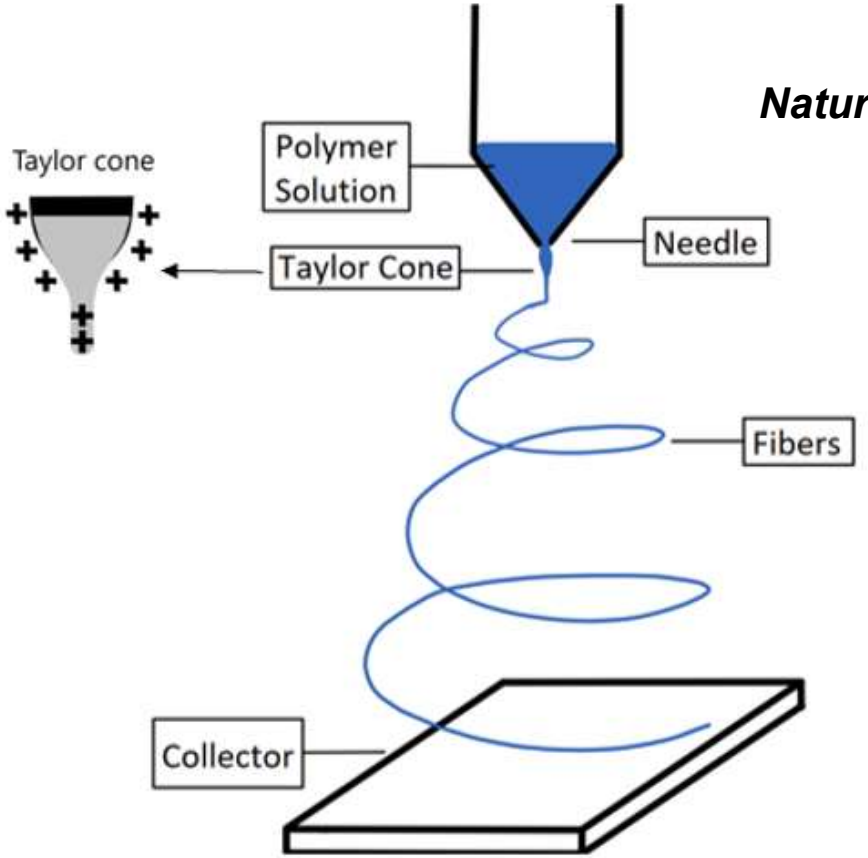


- **The key to revolutionize advanced technologies is to develop affordable and reliable nanomaterials**

- **Thus, materials fabrication routes and sensor design should be upgraded to industrial scale**

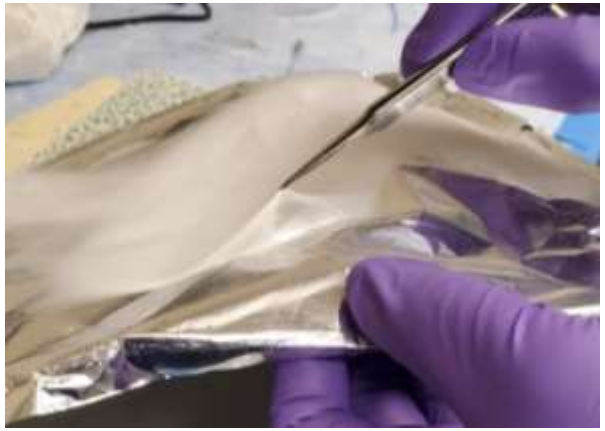
Ceramic Electrospinning

- Fiber processing technique
- Dissolved solution of polymer and/or other materials with volatile solvent
- Electrostatic repulsive force of E-field overcomes surface tension of solution
- Taylor cone forms
- Fibers accelerated towards collector



Schematic of electrospinning process

***Nature Scientific Reports* 14, 2584, 2024**



Nonwoven fibrous mat via electrospinning

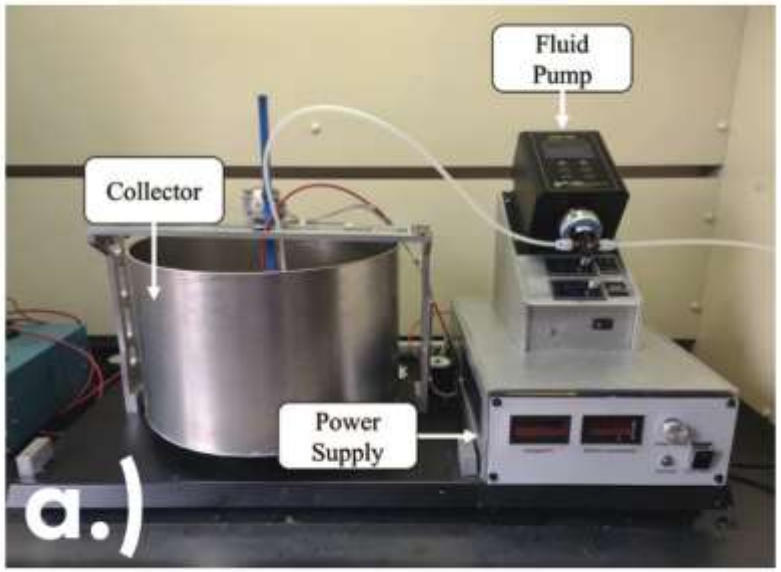
Article | Open access | Published: 28 October 2024

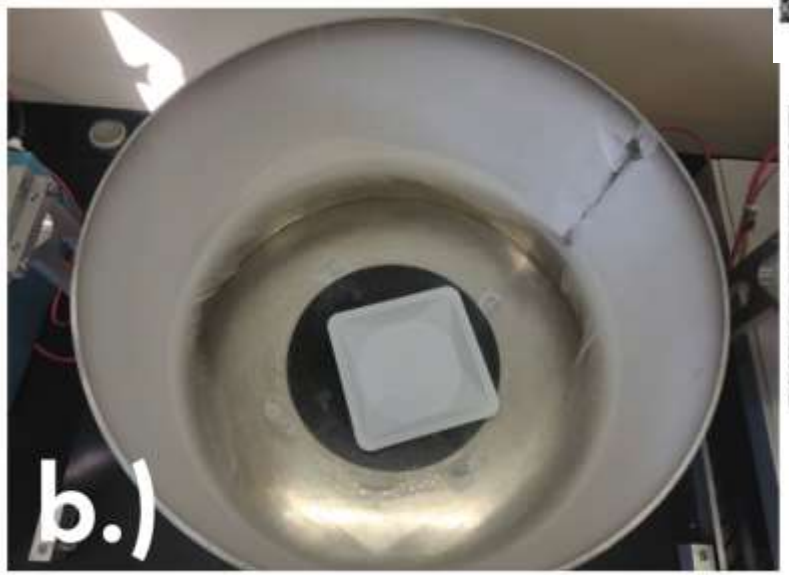
Scalable electrospinning using a desktop, high throughput, self-contained system

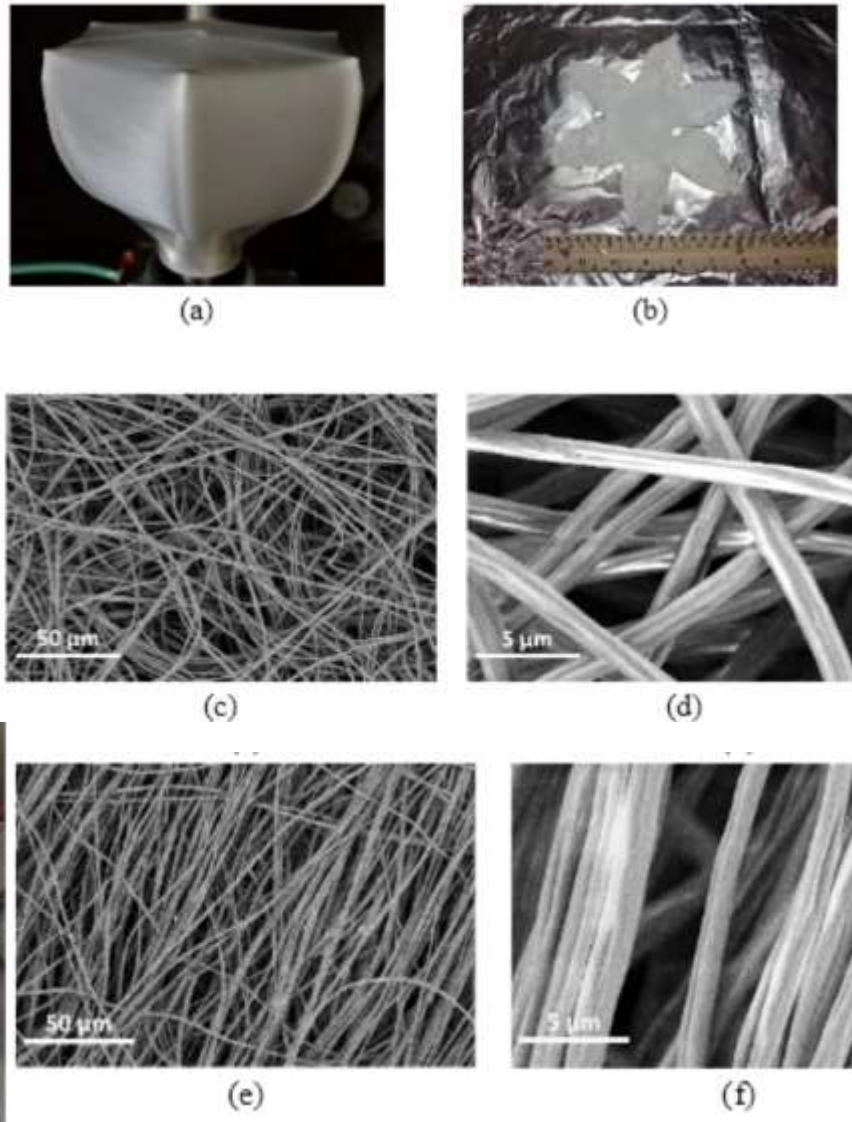
Tessa S. Gilmore & Pelagia-Irene Gouma

Scientific Reports **14**, Article number: 25844 (2024) | Cite this article

6941 Accesses | **5** Citations | Metrics







Sample on rotating collector.

Visible Light-Activated and Self-Supported Electrospun Photocatalytic Nanogrids

- **Oxide-based Photo-assisted Oxidation is a Most Promising Route to Effective and Eco-friendly Decomposition of Hydrocarbons in Water**

- **Visible-Light Activated Electrospun Photocatalysts are also the Most Promising Materials for Photochemical Water Splitting**

I. Utilizing Solar Energy to Clean up Pollutants-
The Role of Semiconducting Oxide Photocatalysts

- **Photocatalytic decomposition of organic pollutants in water** is receiving increased attention in recent years as it **involves reactions utilizing solar energy**

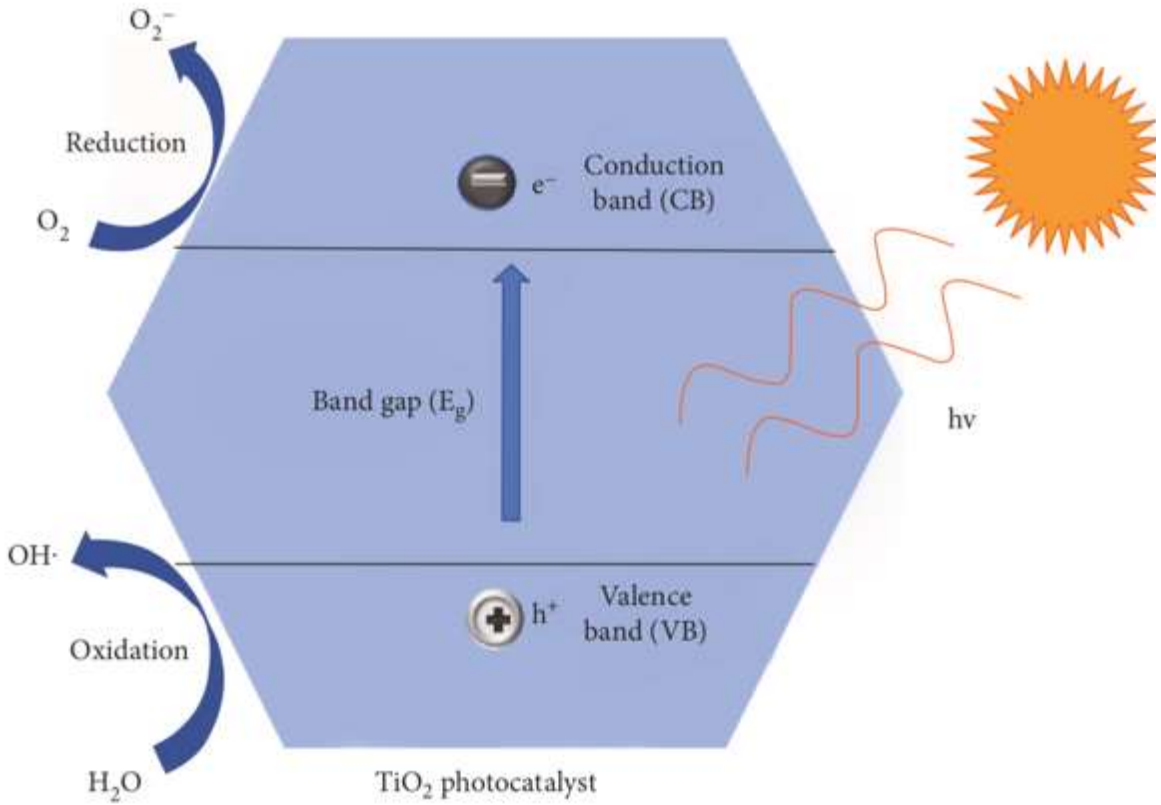
- Specifically, n- type semiconductors, such as titania (TiO_2), when illuminated with light having a higher energy than the semiconductor's band gap are capable of decomposing organic compounds

- **Photocatalytic oxidation:** ***"a free-radical catalyzed thermodynamically spontaneous process… that proceeds at ambient temperature"***
- The hydroxyl radicals initiate the oxidation of hydrocarbons to carbon dioxide, water, and water-soluble organics (aldehydes, ketones, phenolates, carboxylates) products that may "rapidly biodegrade by marine bacteria" through the **photocatalytic oxidation reaction:**

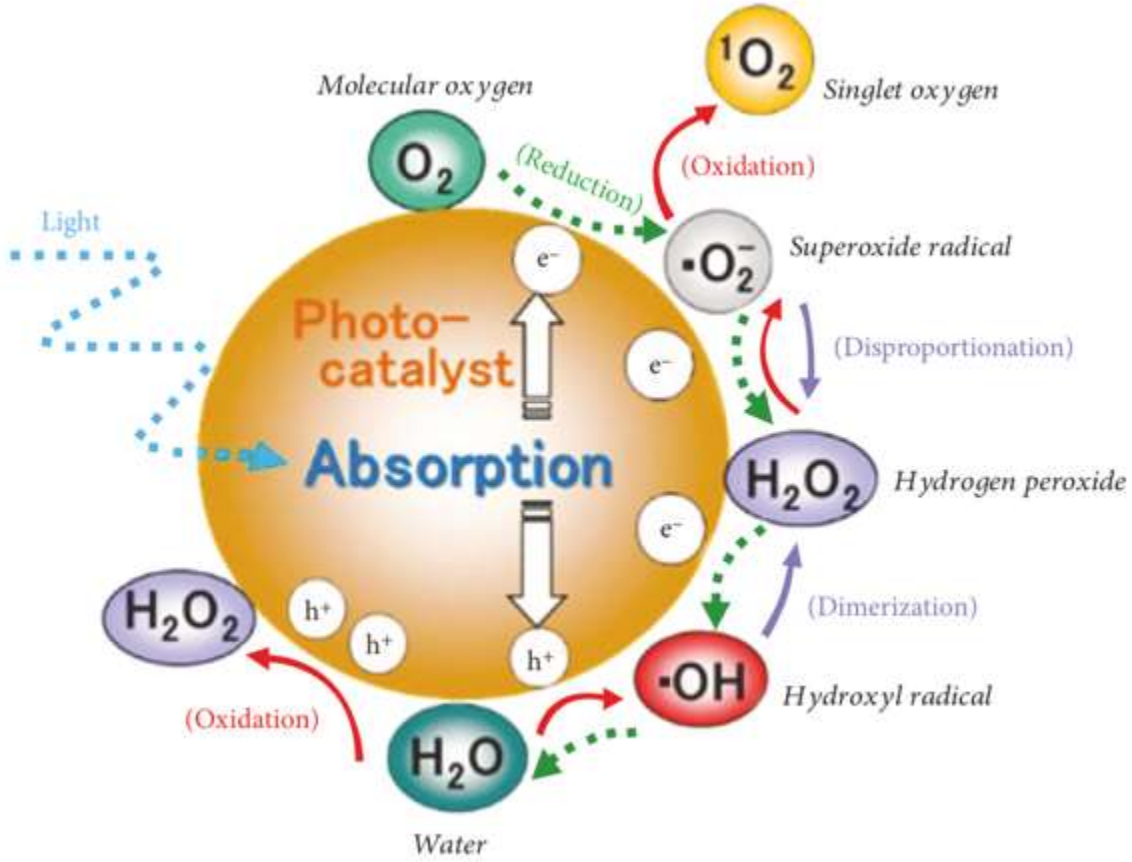
$$RCH2CH2R' + 'OH \rightarrow R6HCH2R' + H,O$$

(*Ind. Eng. Chem. Res.*, 32, pp. 2318-2323, 1993)

Schematic of the Operating Mechanism for Semiconductor Photocatalysis



The Basic Operating Mechanism of a Semiconductor Photocatalyst



Production of reactive oxygen species by chain reaction (reprinted with permission from Nosaka and Nosaka, Chemical Reviews, vol. 117, no. 17, pp. 11302–11336, 2017)

Limitations of Pure Titania as a Photocatalyst

- "approximately 96.0-97.0% of the sea-level solar irradiance consists of photons that are not sufficiently energetic to promote valence band electrons to the conduction band of TiO_2 (anatase)"
- Electron-Hole recombination is on the order of < 30ps, hence efficiency is low (< 5%)



A typical UV light installation for wastewater treatment using titania photocatalysts is shown here

Note the need to *use UV lamps* and to also *build a filtration system* to contain the *dispersed particles* of the photocatalyst

Source: Water Quality Association

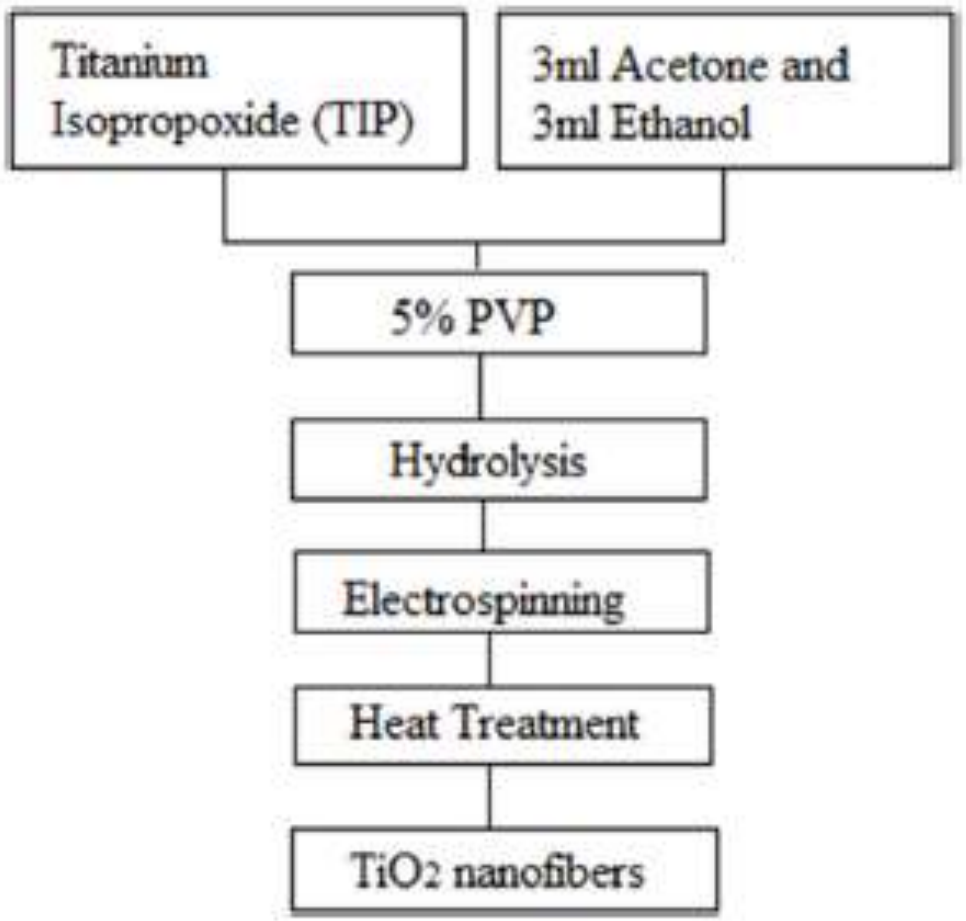
OUR WORK MADE BOTH OF THESE REQUIREMENTS OBSOLETE

Self-supported Mixed-phase Titania Photocatalysts

- Non-woven fibrous mats
- Self-supported nanocatalyst configurations
- Interwoven anatase and rutile or "catalytic 'hot-spots'
- Easily recovered following photocatalytic action

Sample	Phase content (%)		Crystalline size (nm)	
	Anatase	Rutile	(101) Anatase	(110) Rutile
TiO_2-450°C	100	–	7.08 ± 1.1	–
TiO_2-500°C	90	10	15.52 ± 3.1	20 ± 3.0
TiO_2-600°C	84	16	19.8 ± 4.1	24 ± 2.0
TiO_2-700°C	57	43	30.7 ± 5.2	32 ± 5.0
P25	75	25	24.4 ± 3.0	35 ± 3.0

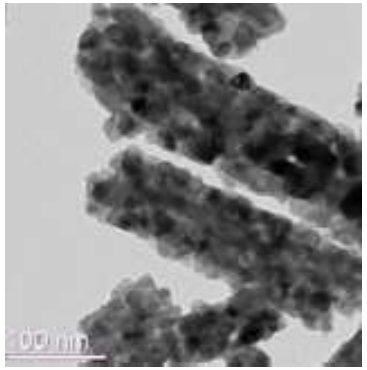
BLEND ELECTROSPINNING

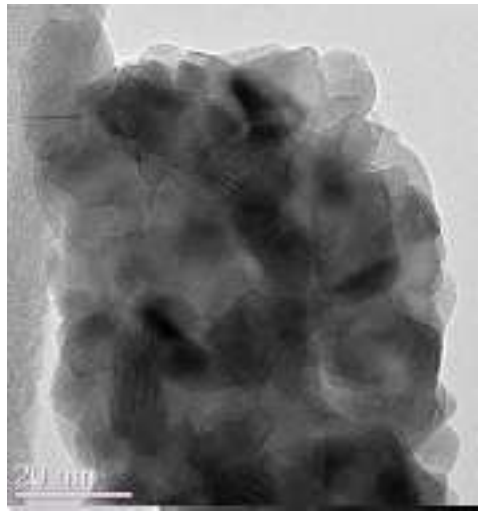


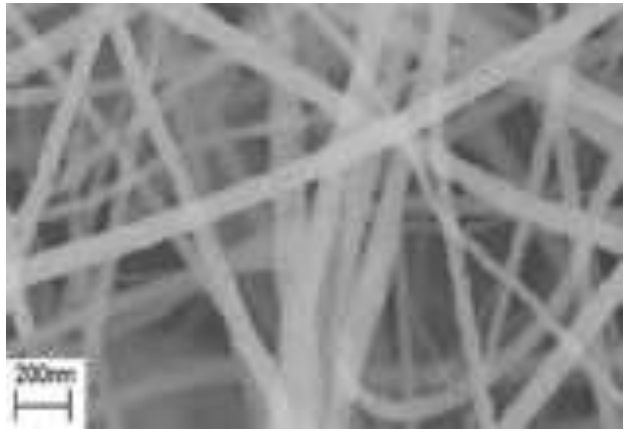
***Front. Mater.*, 21 July 2016**

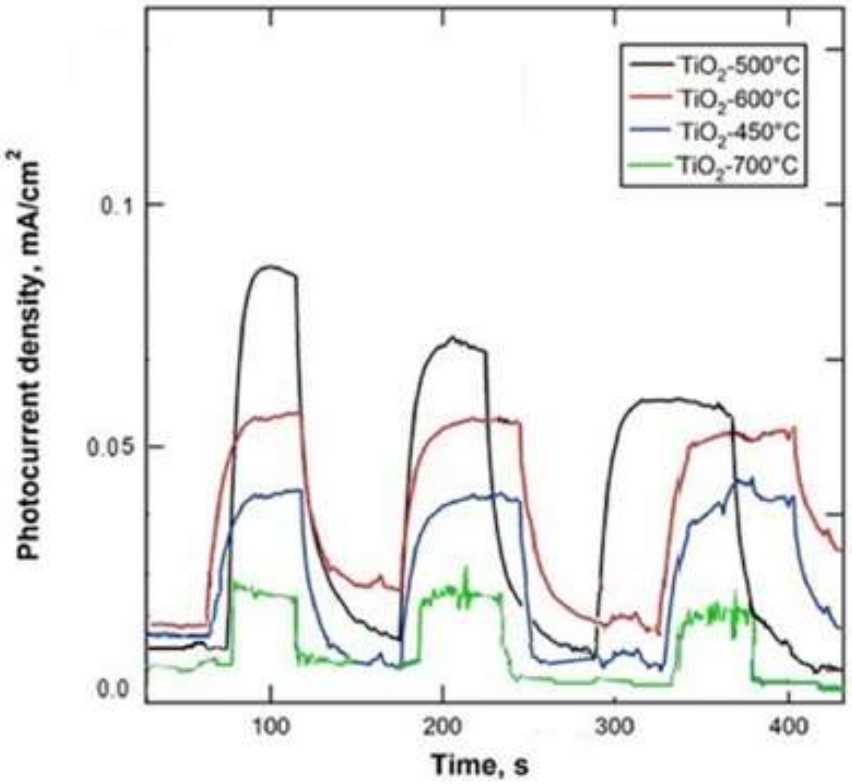
OPTIMIZED TiO_2 NANOSTRUCTURE

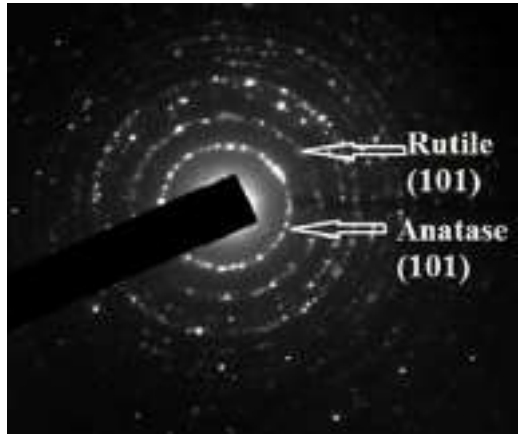
- Optimum Photocatalytic Activity : **A:R ratio 90:10**; particle size: 15-20nm
- Defect-like contrast on anatase grains due to rutile lath formation
- Shear process mechanism described before by Gouma & Mills 2001
- Synergistic effects of two phases occurring on transforming anatase grains











OUR ELECTROSPUN TITANIA PHOTOCATALYST IS MORE EFFICIENT THAN THE COMMERCIAL DEGUSSA P-25

Photocatalysts Produced in this Work

TiO_2	Electrospinning/ Sol Gel (Fibers)	Ti Isopropoxide	Fully degraded MB
WO_3	Electrospinning/ Sol Gel (Foams)	W Isopropoxide	Visible Range photocatalysis
CuO-TiO_2 Composite	Electrospinning/Sol Gel (Fibers)	Ti Isopropoxide Cu Nitrate	Visible Light activated Fully degraded MB and AZO Dyes
CuO-$CuWO_4$ Composite	Sol Gel (Particles)	W isoporpoxide 5% w/v Cu2O powder	Fully degraded MB and Benzene, AZO Dyes
Ce Doped-TiO_2	Electrospinning/ Sol Gel (Fibers)	Ti Isopropoxide Ce Isopropoxide	Fully degraded MB
Cu Doped-TiO_2	Electrospinning/ Sol Gel (Fibers)	Ti Isopropoxide Cu Nitrate	Fully degraded MB

Topcu, Selda, Gagan Jodhani, and Perena Gouma. "Optimized nanostructured TiO2 photocatalysts." *Frontiers in Materials* 3 (2016): 35

Jodhani, Gagan, et al. "Self-Supported Nano-WO3 Foams formed by Self-Assembly of Non-Woven Mats." *Journal of Advances in Nanomaterials* 1.2 (2016): 57

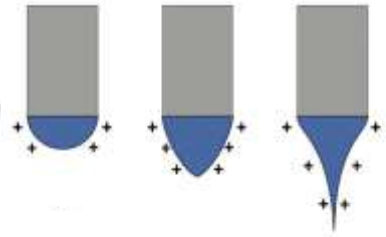
Pawar, Milind, S. Topcu Sendoğdular, and Perena Gouma. "A Brief Overview of TiO2 Photocatalyst for Organic Dye Remediation: Case Study of Reaction Mechanisms Involved in Ce-TiO2 Photocatalysts System." *Journal of Nanomaterials*2018 (2018)

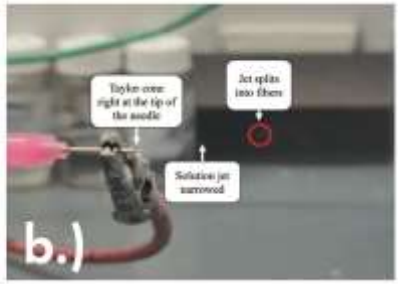
ACS Publications
Most Trusted. Most Cited. Most Read.

Crystal Growth & Design > Vol 24/Issue 16 > Article

Subscribed

ARTICLE | August 1, 2024

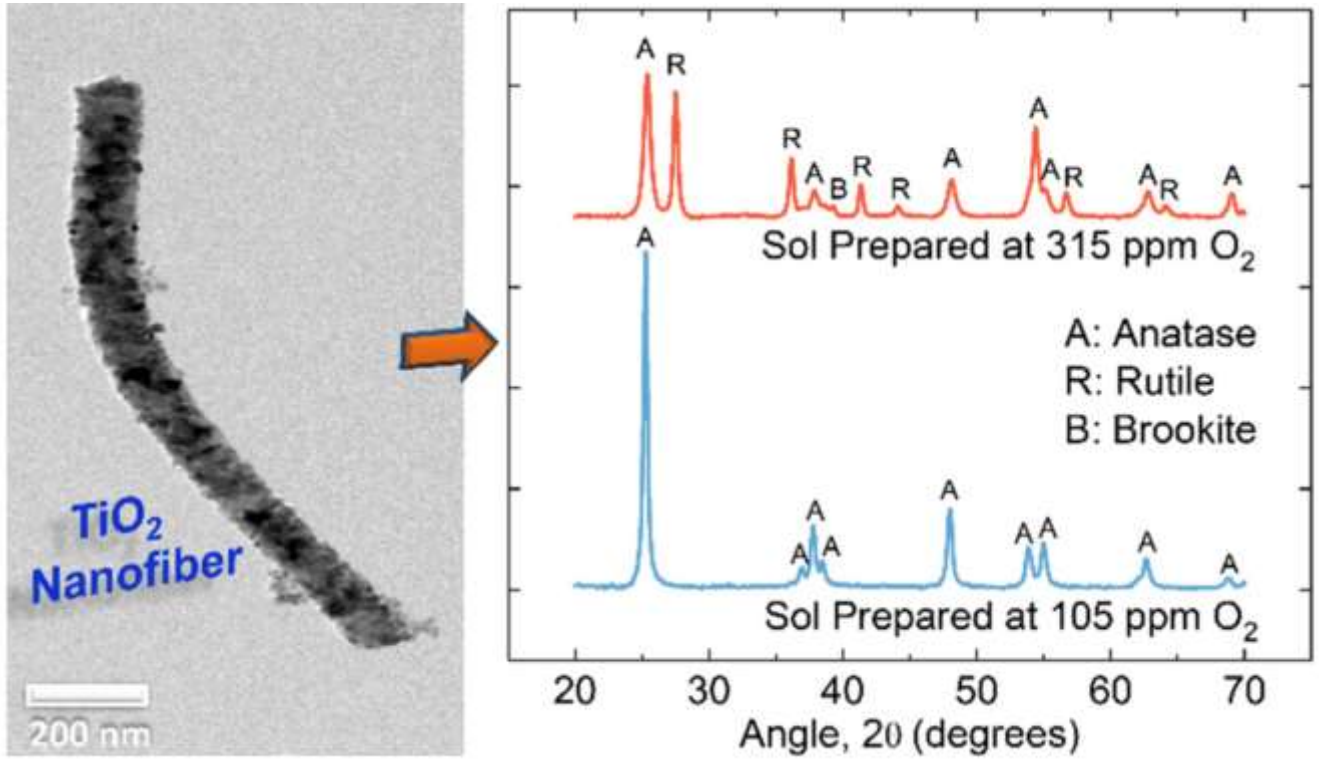


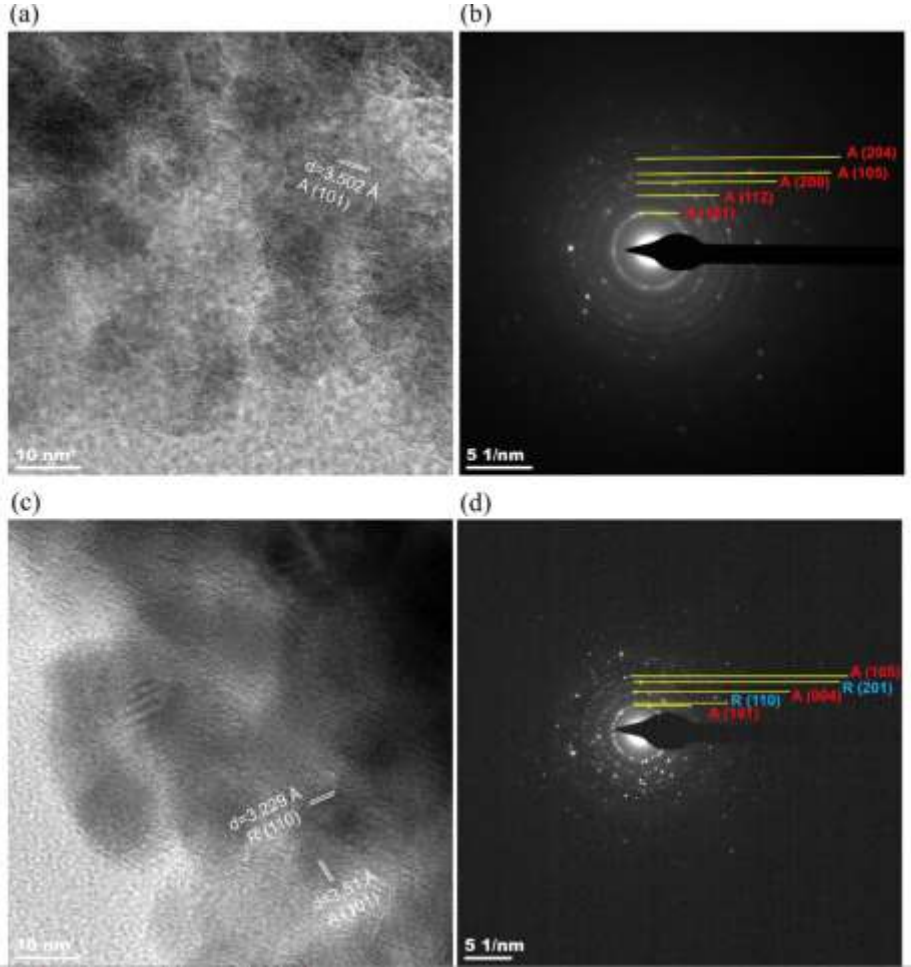




Oxygen Level Controlled Polymorphic Transformation in Sol–Gel Processed Electrospun TiO_2 Nanofibers

Mohammad Mahafuzur Rahaman, and Pelagia-Irene Gouma*



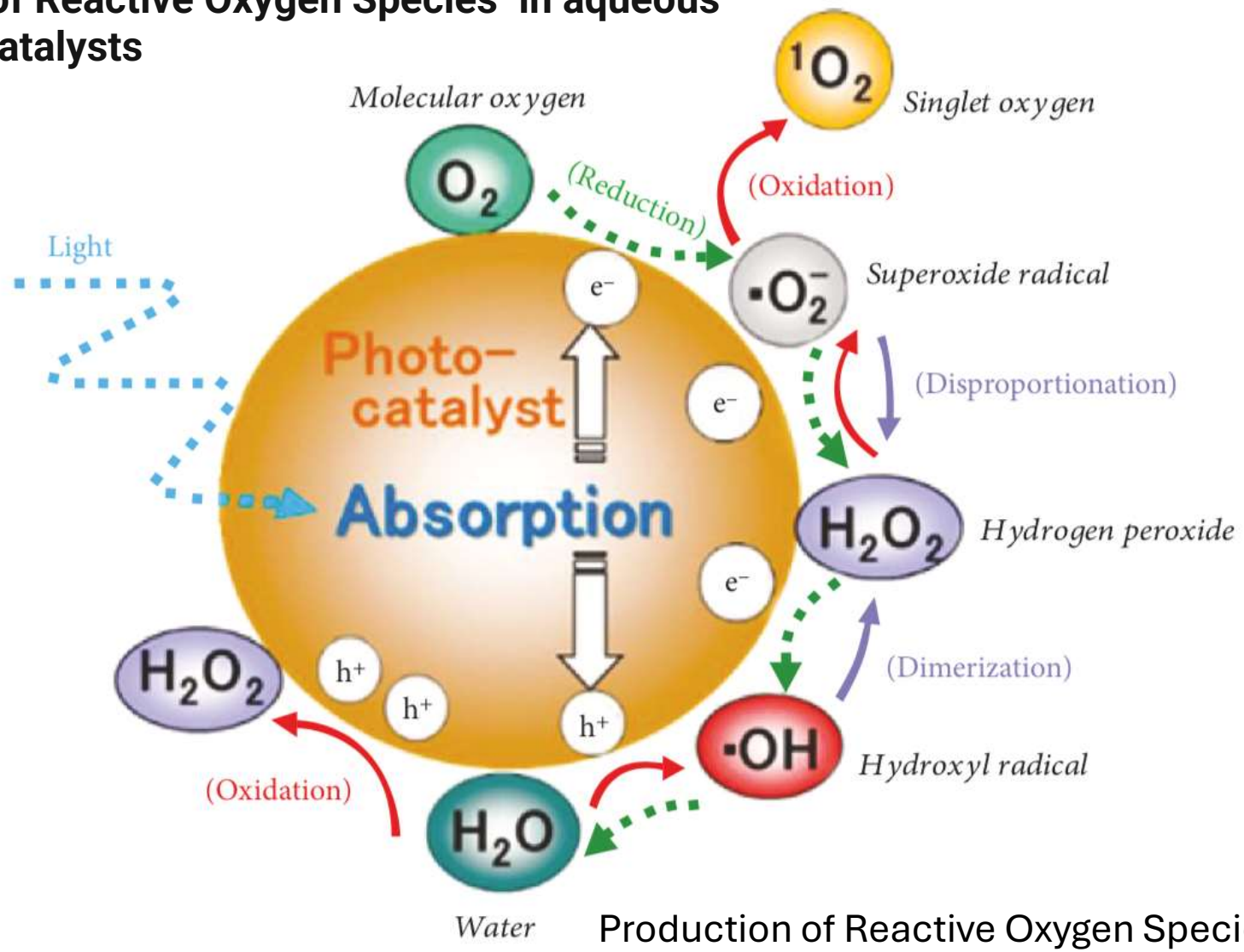


Generation Reactions of Reactive Oxygen Species in aqueous suspensions of photocatalysts

The species to which oxygen converts with high reactivity are called reactive oxygen species (ROS)

Major ROS:
superoxide anion radical (•O2−),
hydrogen peroxide (H_2O_2),
singlet oxygen ($^1O2$), and
hydroxyl radical (•OH)

ROS are also important for advanced oxidation processes, e.g. to remove organic pollutants in the wastewater



Production of Reactive Oxygen Species by Chain Reaction

Nosaka and Nosaka, Chemical Reviews, vol. 117, no. 17, pp. 11302–11336, 2017

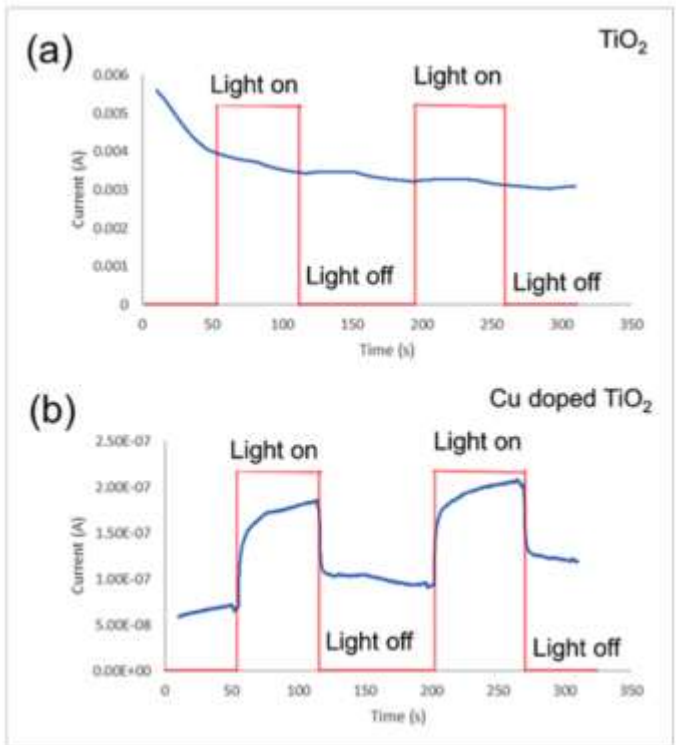
ADVANCED SCIENCE

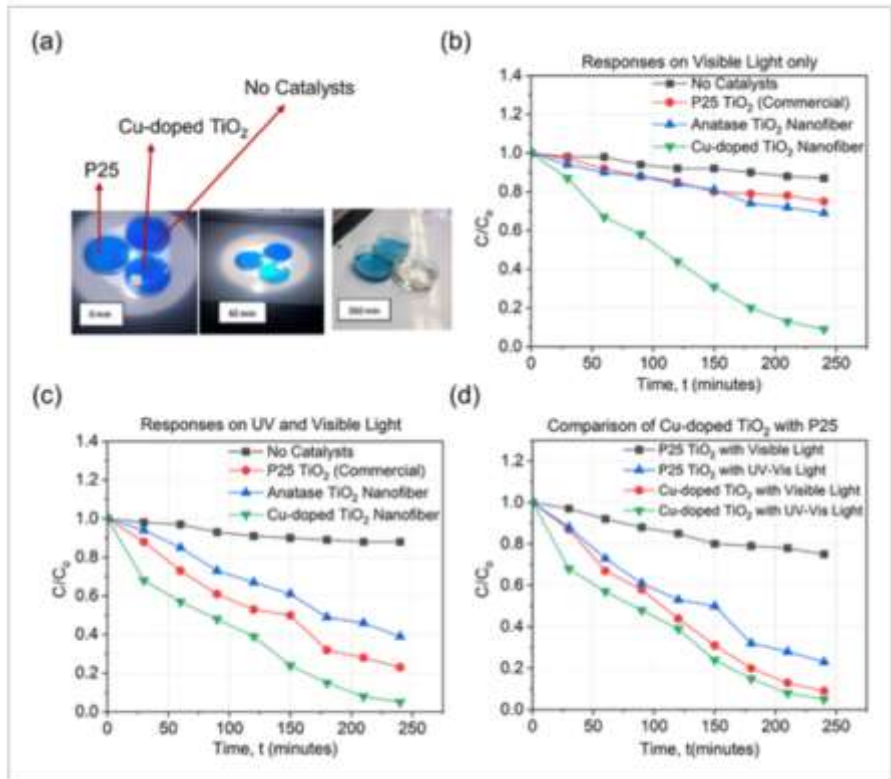
Research Article | Open Access

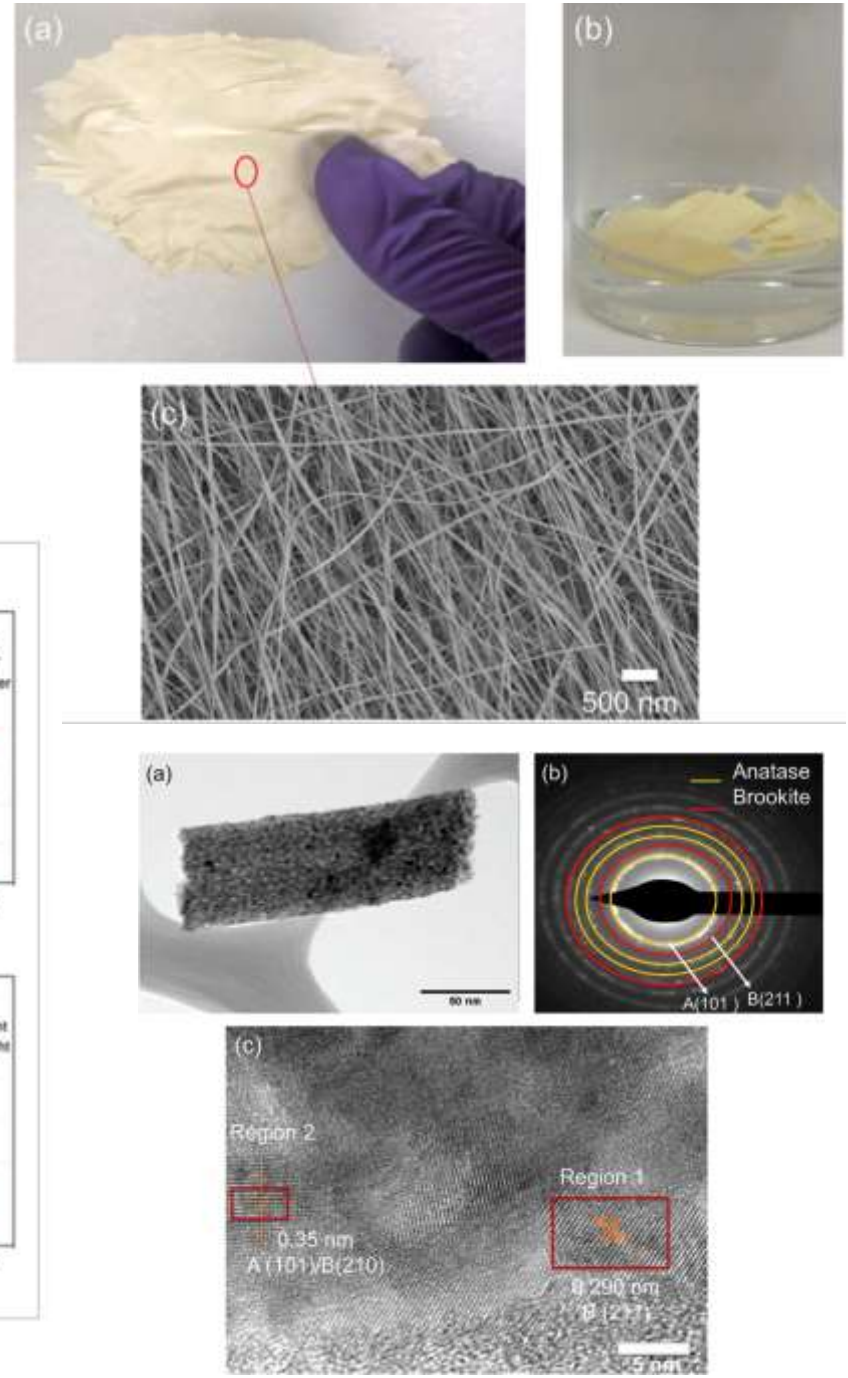
3D Self-Supported Visible Light Photochemical Nanocatalysts

Fateh Mikaeili, Mohammad Mahafuzur Rahaman, Pelagia-Irene (Perena) Gouma

First published: 24 March 2025 | https://doi.org/10.1002/advs.202502981 | VIEW METRICS







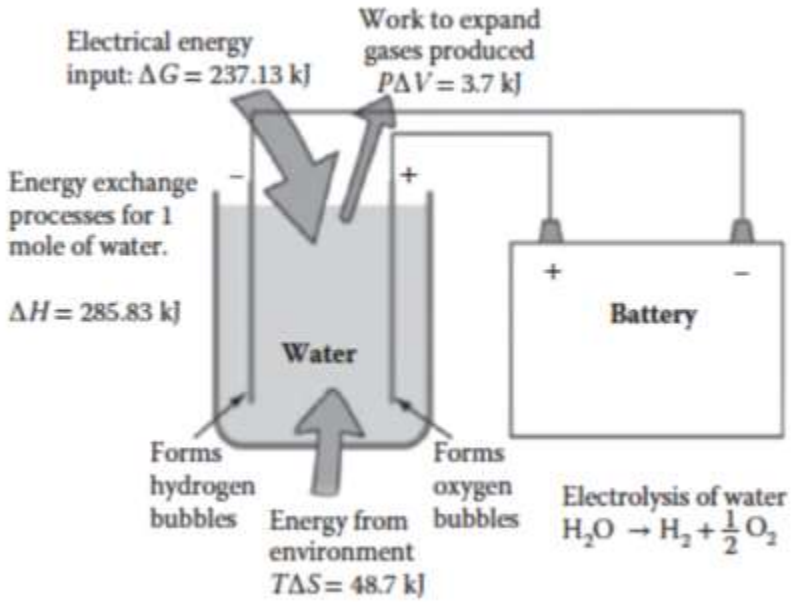
a,b) Chronoamperometry of undoped and Cu-doped TiO_2 nanofibers, respectively.

Our Photocatalysts in Action

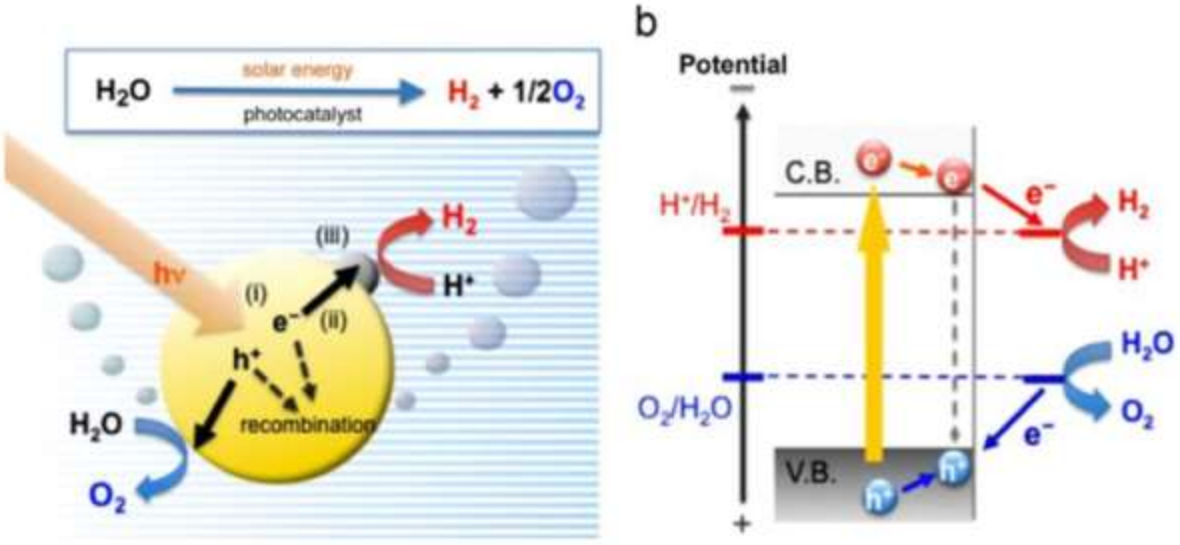


Utilizing Photocatalysts for Solar Water Splitting

Combining Solar energy with the Plentiful Water Resources and a Catalyst to Produce Hydrogen Fuel



Thermodynamics of Water Splitting



Solar Photocatalytic Water Splitting

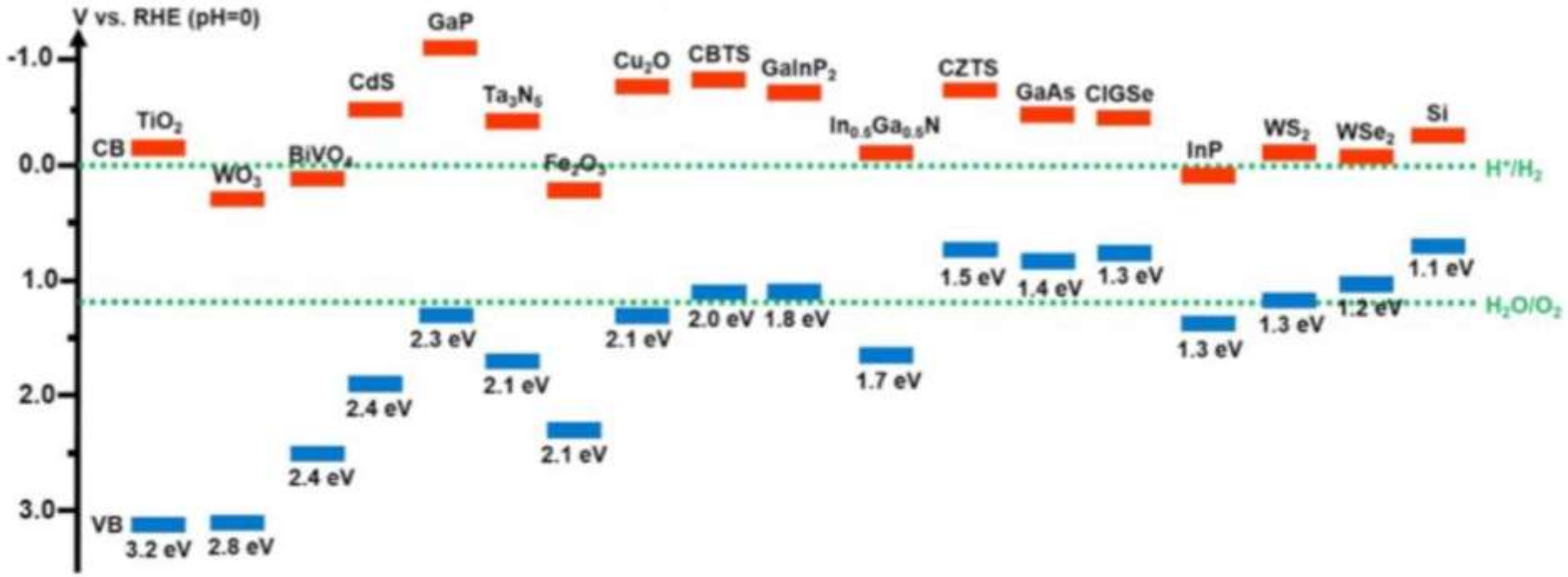
Overall reaction:

$$2H_2O(l) + 4e^- + 4h^+ \rightarrow O_2(g) + 2H_2(g) \quad E = -1.23\ \text{V versus NHE}$$

where NHE is the normal hydrogen electrode.

Criteria for selection and synthesis of the ideal photocatalytic material

- Chemical and Electronic properties of the material
- Physical Properties and Crystal Structure of the material
- Overcoming current limitations in efficiency, stability and scalability



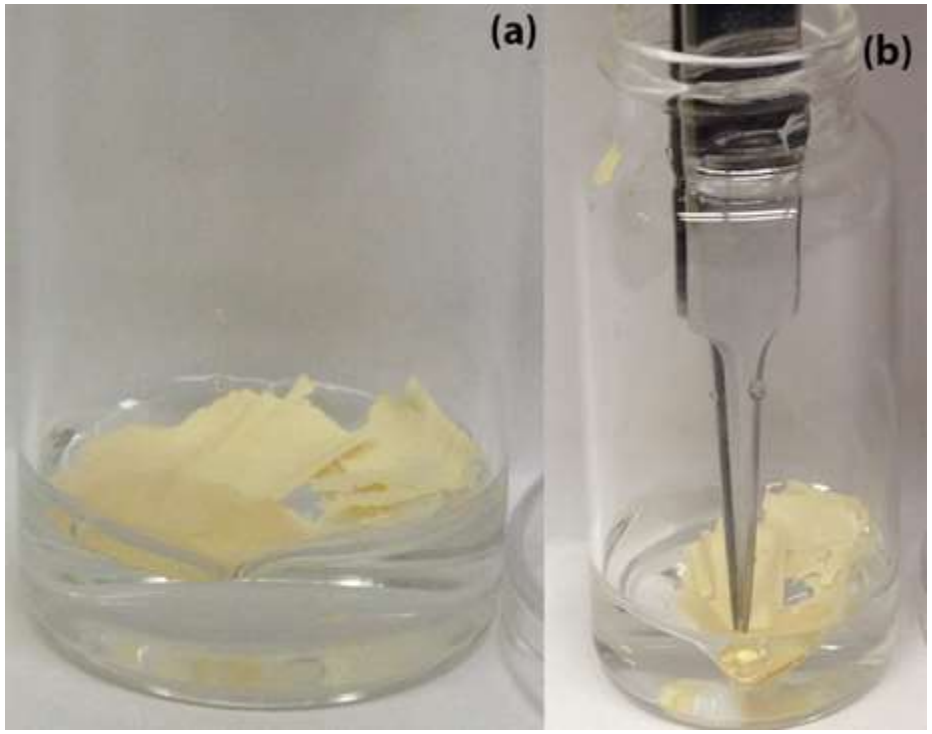
Key requirement for one-step water splitting catalysts is that their CB edge and VB edge should straddle the $H+/H_2$ and O_2/H_2O redox potentials

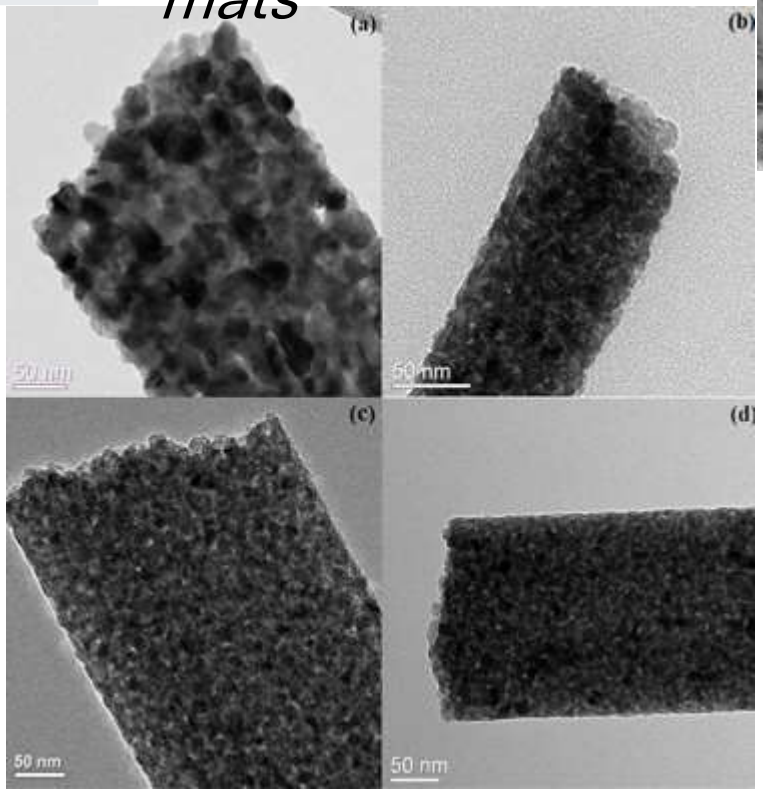
Visible-Light Activated Oxide Photocatalytic Nanogrids™

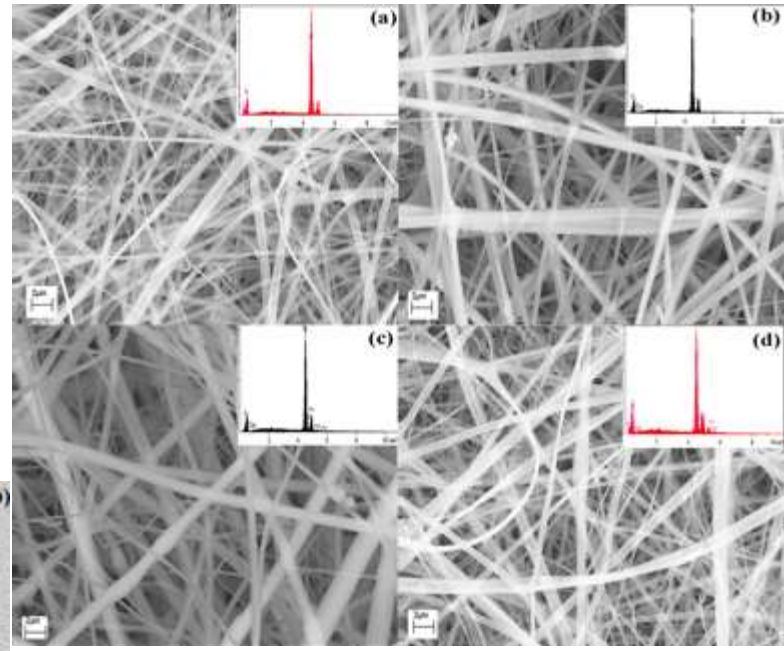
Cerium as a dopant in aqueous phase photocatalytic reactions

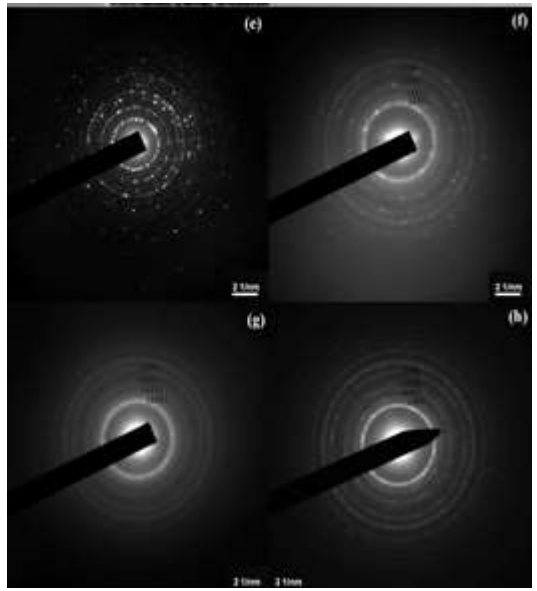
Sample	Ce content (Atomic Weight%)	% Anatase	% Brookite
CE0	0	89	-
CE1	1	87	12
CE3	3	80	20
CE4	4	77	23

Cerium-doped TiO_2, 3D, ***self-supported,*** *Electrospun, photocatalytic mats*

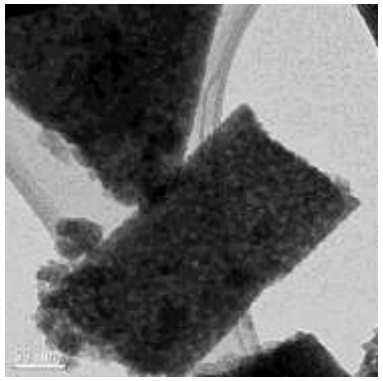


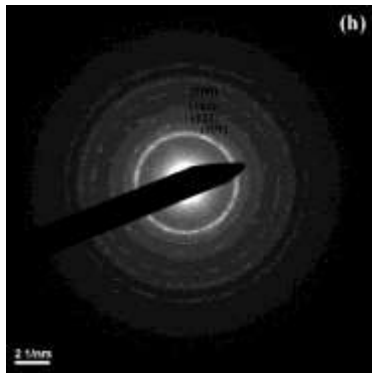


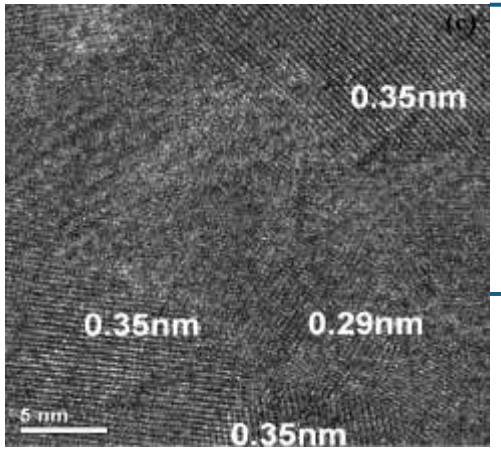




Un-assisted Photocatalytic Water Splitting for Hydrogen production using electrospun mats of the Ce-TiO_2 system







Morphology and Crystal Structure of the electrospun and calcined mats as seen in TEM

- The 3% Ce doped Titania nanomats had the best photocurrent density (0.32mA/cm^2) reported to date for the Ce-TiO_2 system
- Their band gap energy is 2.32 eV



High –throughput processed Photocatalytic mat



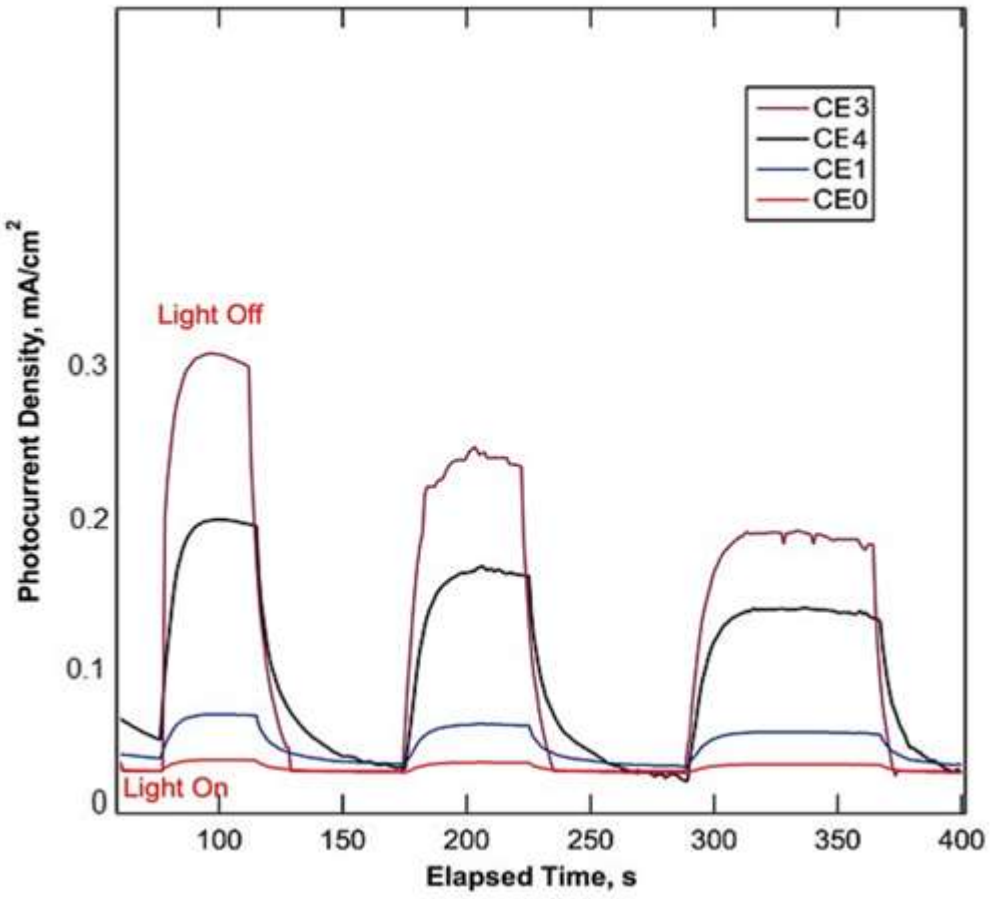
Water splitting experiment



- These are self-supported mats that float on water
- On exposure to sunlight they result in un-assisted photocatalytic water splitting

S. Topcu, Ph.D.thesis, Stony Brook, 2016

Photocatalytic Properties of Ce-TiO_2 Nanogrids™



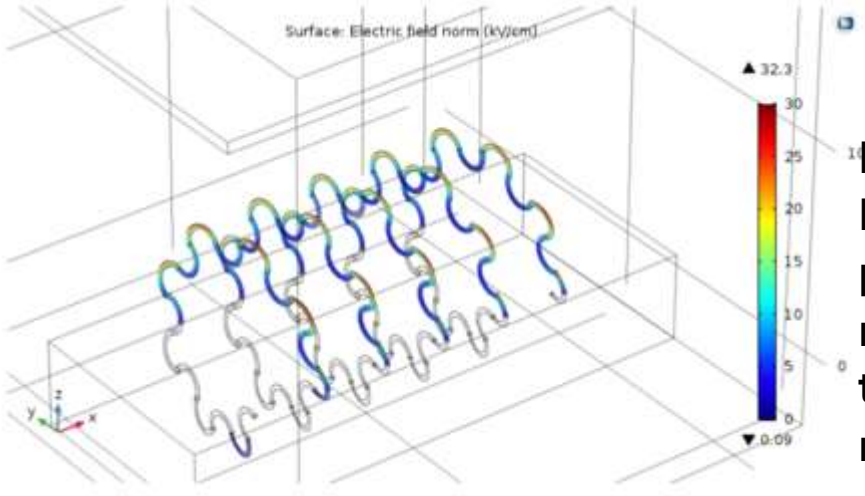
Chronoamperometry curve of CE0, CE1, CE3 and CE4 Ce-TiO_2 nanofibers mats annealed at 500^0C – in 0.1M KOH solution; Scan rate: 20mV/s

Materials	mol/weight%	Structure	Reactant solution	Scan rate	PhotoCurrent density	Ref.
TiO_2		Nanofibers	1M KOH	10 mV/s	0.15 mA/cm²	[1]
TiO_2/CeO_2	2%Ce	Thin Film Nanoparticle	Na_2SO_4 0.5 M Ag/AgCl/Cl^- Platinum	25mV/s	0.02 mA/cm²	[2]
$Ce/RGO/TiO_2$	1wt%Ce+ 1wt%RGO	Nanoparticle	0.1M Na_2SO_4 (SCE) Platinum	50mV/s	0.74mA/cm²	[3]
TiO_2 P25 TiO_2/CeO_2	2% Ce	Thin Film Nanoparticle	0.5 M Na_2SO_4 Ag/AgCl/Cl^- Platinum	25 mV/s	0.15mA/cm² 0.22mA/cm² 0.12mA/cm²	[4]
TiO_2/CeO_2	0.5wt% Ce	Thin Film	Na_2SO_4 0.1 M +0.1 M H_2SO_4 (ph:4)		0.3mA/cm²	[5]
TiO_2		Nanofiber	0.5 M Na_2SO_4		0.2 mA/cm²	[6
$TiO_2/CeO_2/Au$		Nanotube			0.09 mA/cm²	[7]
TiO_2/CeO_2	3%Ce	Nanofiber	1M KOH	20 mV/s	~0.32 mA/cm²	ours

High-Throughput, Hierarchical, Nano-Manufacturing of Non-Woven ECM-mimicking Scaffolds



High Throughput Electrospinning Set up and 3D non-woven Mats Produced



Oscillating Spiral Coil Spinneret

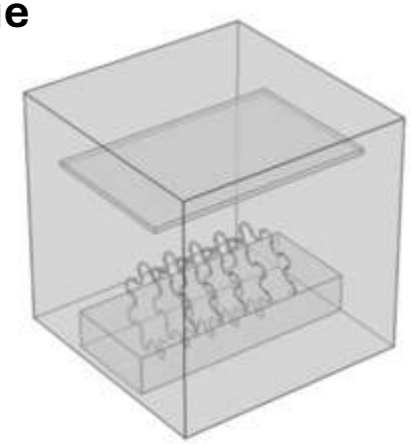
Novel Concept HTES system to produce fiber morphologies that mimic native tissue



The rotation of a spiral spinneret introduces axial "motion" along the surface of the spinneret

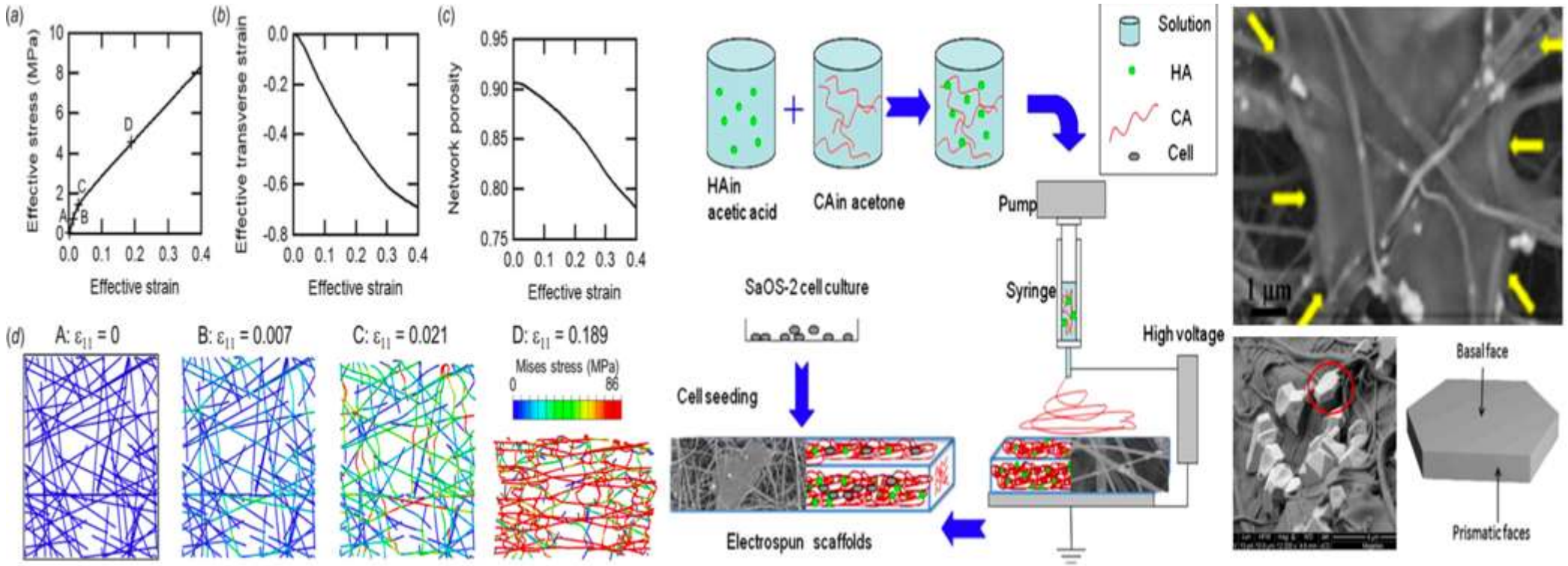
mechanical perturbation has been shown to be an important parameter in electrospinning as it produces wavy fibers

Such fiber morphologies can mimic those of native tissue and can play a role in cell differentiation



Electrospinning apparatus in COMSOL 5.3

Electrospun mats with hydroxyapatite for bone growth



•F. Mikaeili, O. Abe, **P.I. Gouma**, (2022). High Throughput Electrospinning Technologies and Applications (Book Chapter), Advances in Technology and Applications, ASM international ASM Handbook Volume 23A, Additive Manufacturing in Biomedical Applications, 2022, ISBN: 978-1-62708-390-4

•D. Han and **P. I. Gouma**, "Electrospun Bioscaffolds That Mimic the Topology of Extracellular Matrix", in book **"Nanomedicine in Cancer"**, ed. L. P. Balogh, PAN STANFORD PUBLISHING PTE LTD, Singapore, pp. 159-169, 2017

Electrospun constructs for bone and tissue engineering

Novel High-Throughput Spinnerets and Novel Algorithms for controlling the manufacturing to produce fibrous architectures with the desired shape and mechanical properties, and the control over the topology at the microscale open the pathway for the advanced manufacturing of complex 3D tissue scaffolding that will revolutionize the field of regenerative medicine

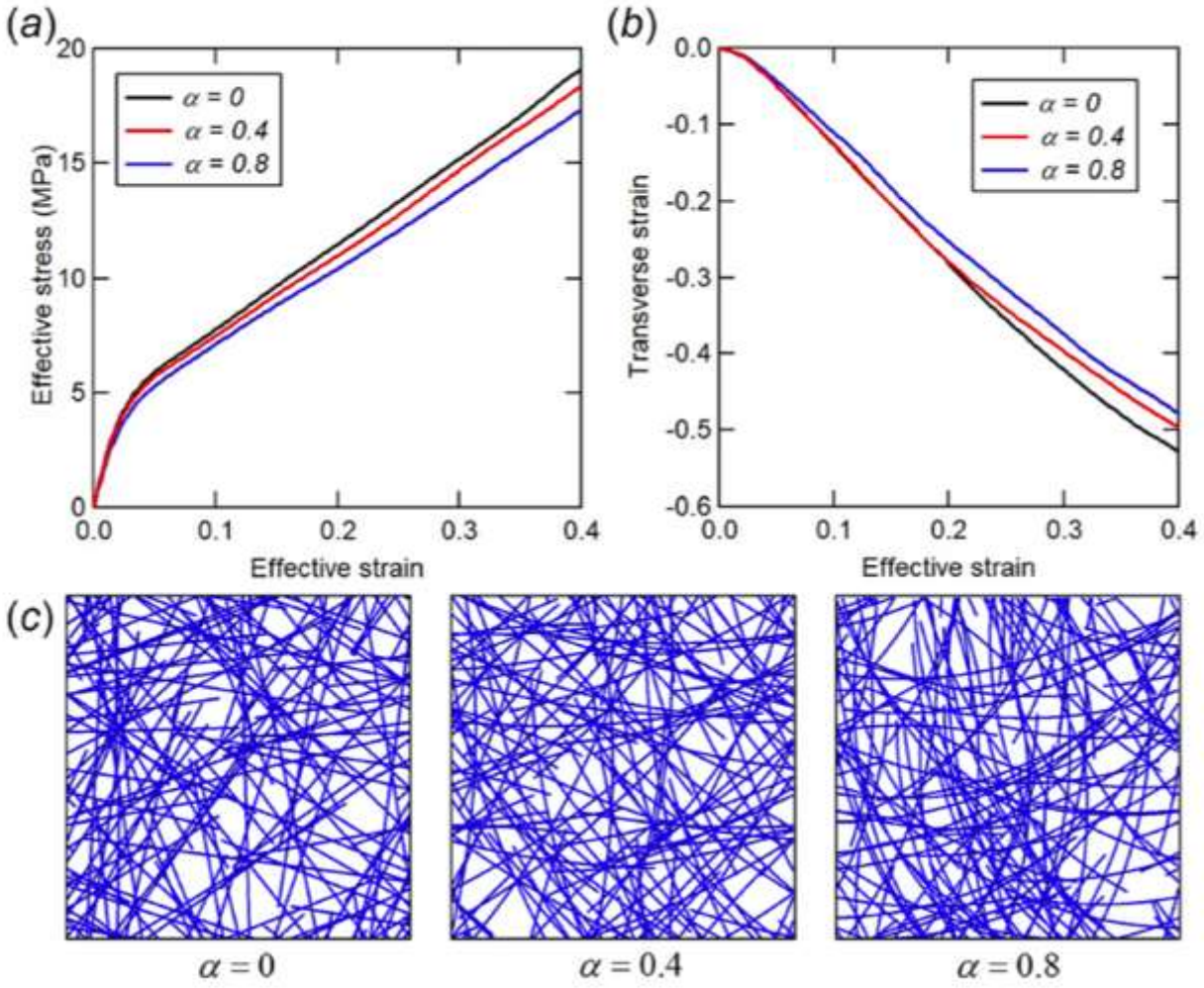


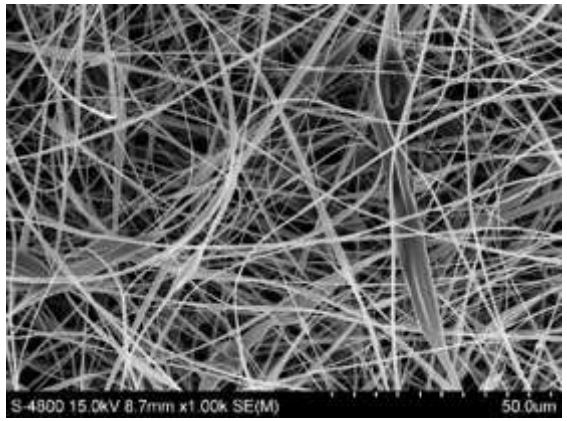
Fig. 11 Mechanical response of random nonwoven fibrous networks with different fiber aspect ratios under uniaxial tensile loading: (*a*) the stress–strain curves with fiber radians of 0, 0.4, and 0.8, (*b*) the effective transverse strain, and (*c*) the schematic diagram of fibrous networks with different fiber radian α

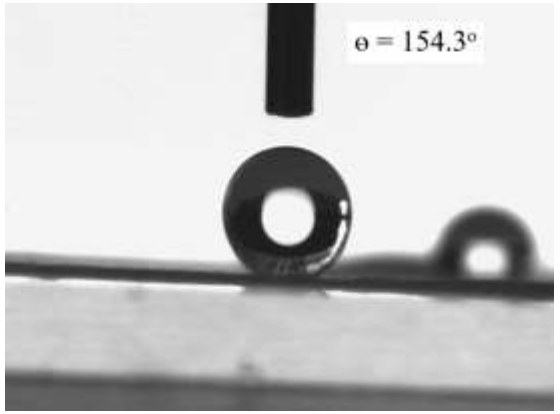
Journal of Applied Mechanics

JANUARY 2019,Vol.86 / 011010-1

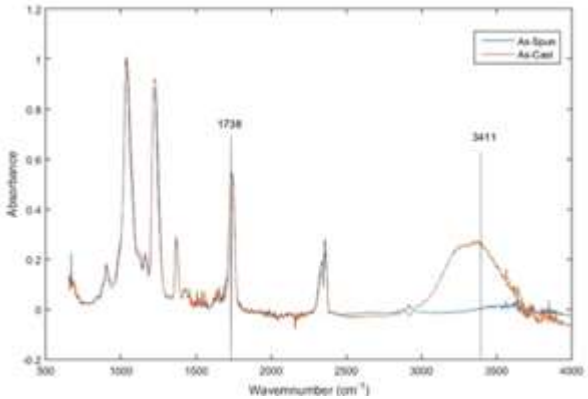
Nanomanufacturing of Biomolecular Materials

Super-hydrophobic CA electrospun mats: In this project, super water repellant CA fibrous mats were developed using electrospinning in one step process without further surface modification. The as-spun CA fibrous mats show low density, high surface roughness, and surface-to-volume ratio (fig. 1). The effect of electrospinning on roughness of the surface was confirmed through applying the Cassie's model on the as-spun fibers, and it is shown that the roughness effect alone in this process cannot induce the shift from hydrophilic to super water repellant.





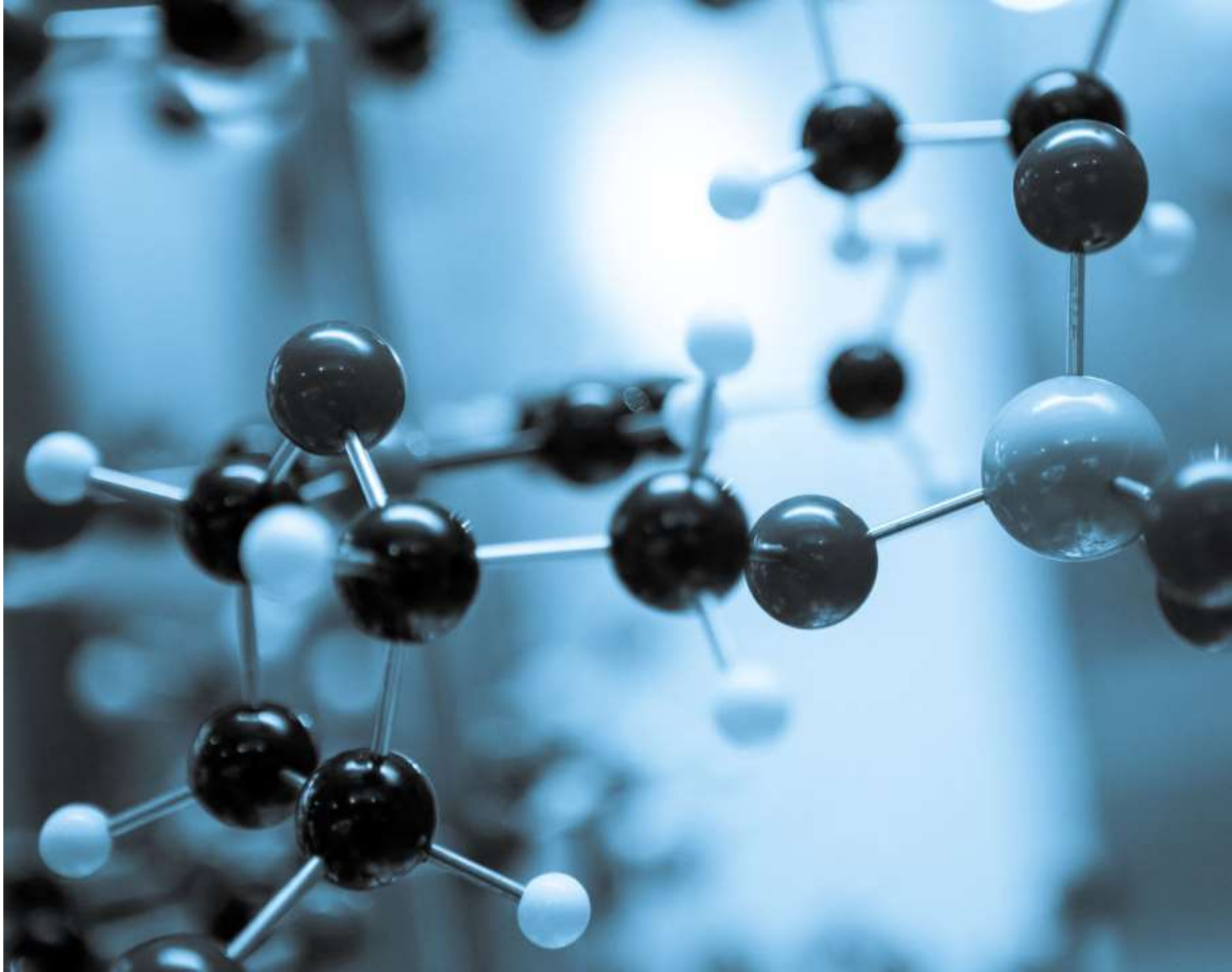




Super water repellant CA fibrous mats were developed using electrospinning in one step without further surface modification. Water droplets on the two sides of the Electrospun CA fiber mat; FTIR analysis shows that the intensity of the hydroxyl band at 3450 cm^{-1} is decreased in as-spun fiber.

T. Gilmore and **P.I. Gouma**, "Electrospinning for Biomaterials Applications", FeatureArticle, ACERS Bulletin, 103(9), 26-32, 2024 (https://digital.bnpengage.com/emagazine-acers-bulletin-december-2024/cover-story-electrospinning/

NEW SCIENCE



Combustion Synthesis of Ceramic Powders

- **Spray pyrolysis:**
  - *Flame spray pyrolysis*
  - *Ultrasonic spray pyrolysis*

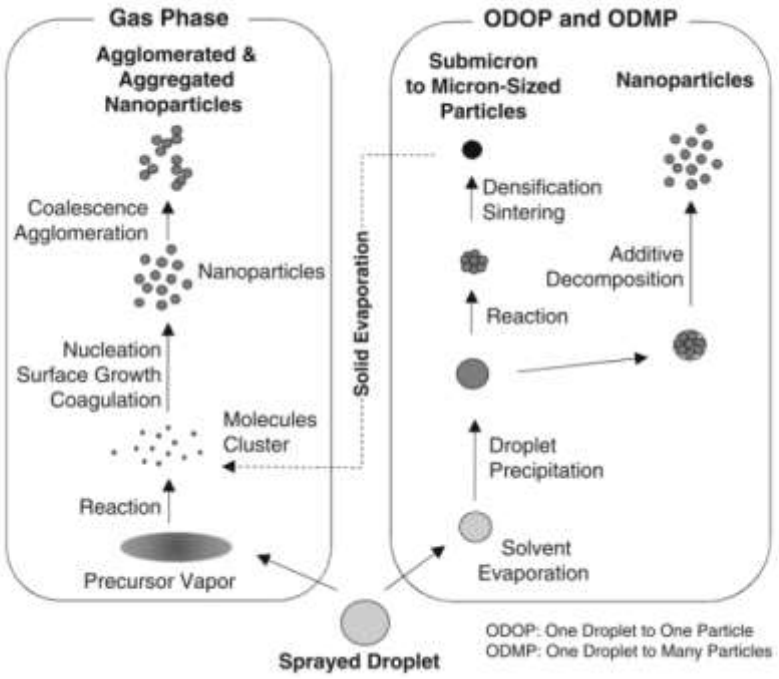


Table 1: FSP parameters that affect the morphology and structure of resulting powders [7].

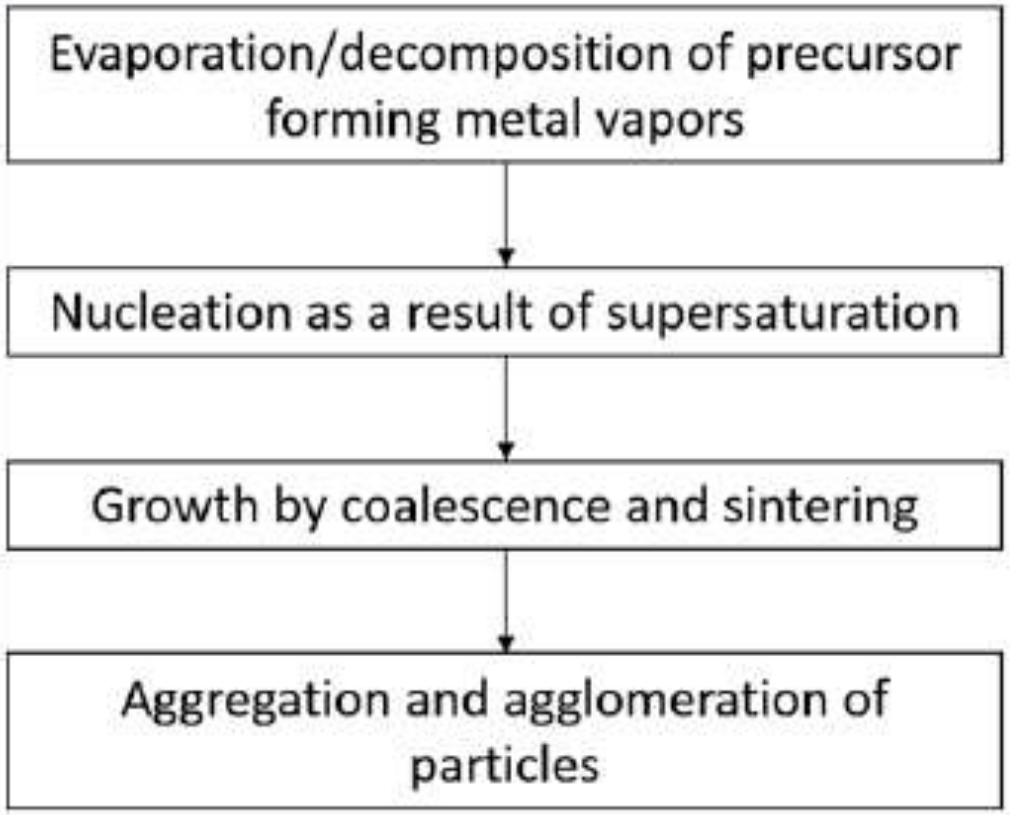
Feature	Controlling Parameters
Crystal size	Precursor composition, fuel and oxidant flow rate, burner configuration, size of droplet and flame
Crystal structure	Precursor flow rate and fuel/oxidant flow rate
Particle Morphology	Precursor concentration and fuel/oxidant flow rate

F. Mikaeili, S. Topcu, G. Jodhani, and **P.I. Gouma**, "Flame-sprayed Pure and Ce-Doped TiO_2 Photocatalysts", *Catalysts*, 8, 342, 2018

G. Jodhani and **P.I .Gouma**, "Flame spray pyrolysis processing to produce metastable phases of metal oxides", **invited paper**, *JOJ Material Science* 1, pp. 1-5, 2017. https://juniperpublishers.com/jojms/JOJMS.MS.ID.555557.php

FLAME SPRAY PYROLYSIS

- The precursor is an organometallic compound
- It evaporates quickly once it enters the flame
- It produces metal vapors
- Particle formation follows
- Homogeneous powders of high purity are made in this process



G. Jodhani, F. Mikaeili, and P**. Gouma**, "Flame Spray Synthesis of $VOPO_4$ polymorphs", *Frontiers in Materials*, 6, 254, 2019

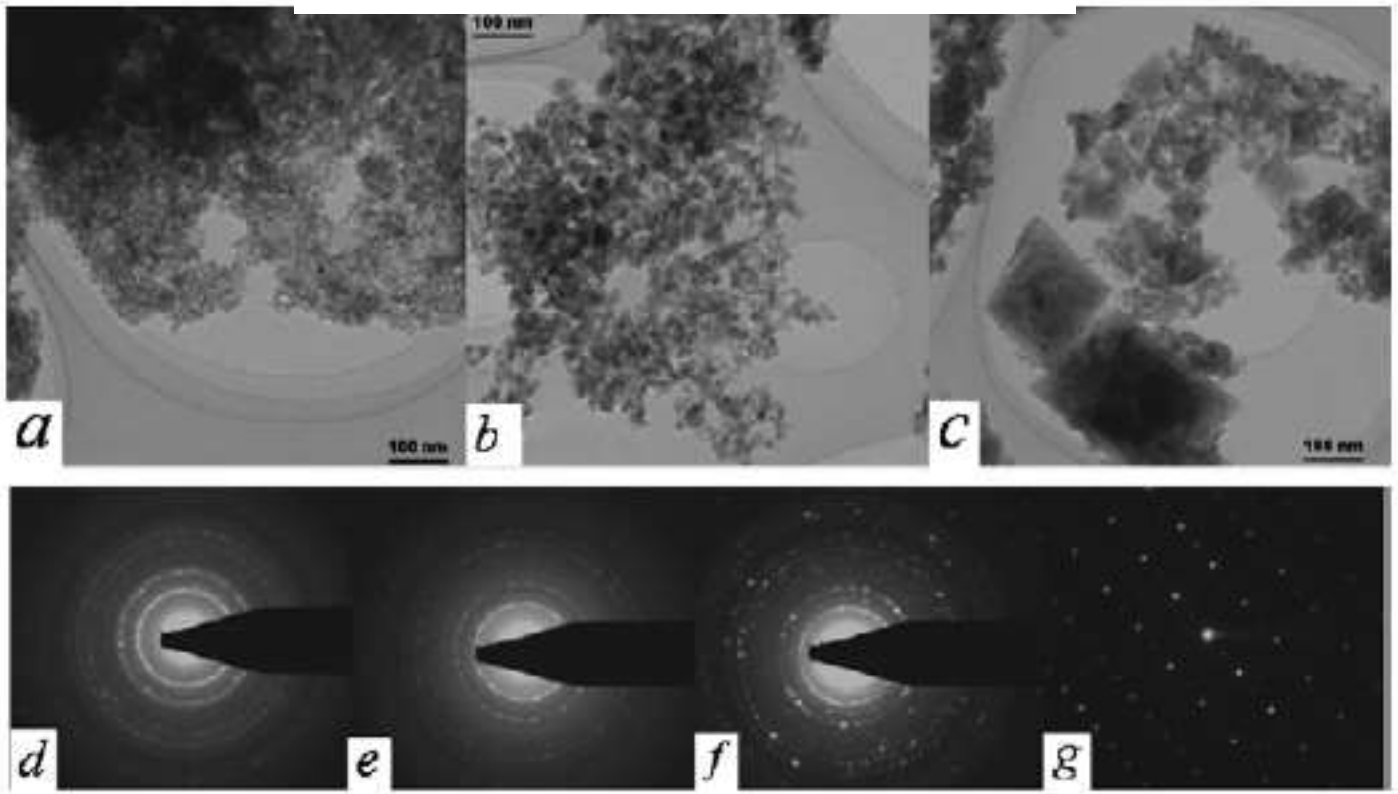
O.O. Abe, G. Jodhani, and **P. Gouma**, "On the coupled ferroelectric-electrochromic effect of epsilon-WO3", *J. Am. Ceram. Soc.*, 101(1), pp. 12-15, 2018

Scalable Process (Flame Spray Pyrolysis)

As-sprayed powders

The as-synthesized powder products resulted from the reaction

$$H_{26}N_6O_{41}W_{12} \xrightarrow{\text{flame}} W^{6+} \xrightarrow{O_2} WO_3$$



Ammonium metatungstate precursor

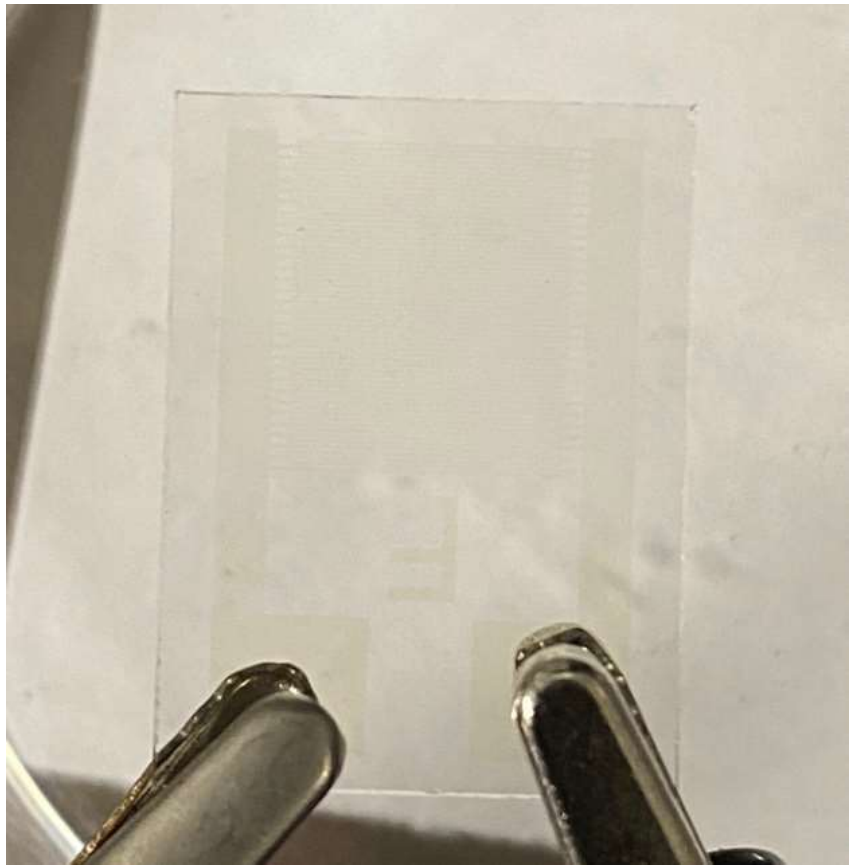
Gouma PI, Wang L (2015) Flame Spray Synthesis of WO_3 for No Breath Monitors. J Material Sci Eng 4: 165. doi:10.4172/2169-0022.1000165

The Novel Phenomenon of Ferrochromism

US Patent number 11,467,459 B2 issued on 10/10/22

ACS Appl. Opt. Mater., 2(4), 604-609, 2024

(a)



(b)



The material is the only self-standing, binary oxide ferroelectric
Ferrochromism has similarities to electrochromism and solvatochromism, but the mechanism is differentiated
Envisioned applications in ubiquitous displays, and novel memories, among others

ACS Applied Optical Materials > Vol 2/Issue 4 > Article

Subscribed

ARTICLE | April 11, 2024

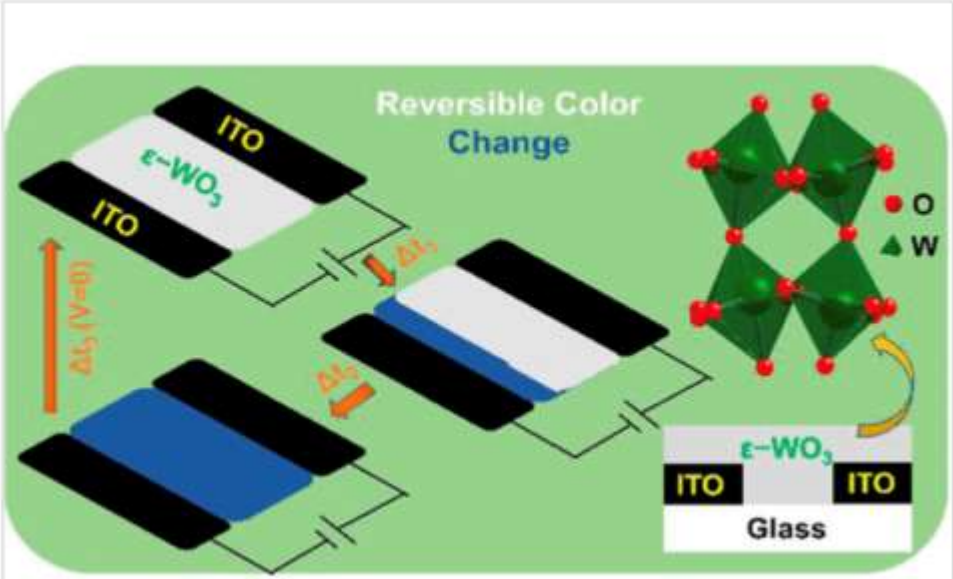
Chromism in Ferroelectric ε-WO_3: Single-Layer Solid-State Color-Changing Devices and Displays

Mohammad Mahafuzur Rahaman*, Anthony Annerino, Jacob Shell, and Pelagia-Irene Gouma

Open PDF | Supporting Information (1) | Find It!

Abstract

WO_3 is well known for its electrochromic γ and hexagonal phases, which are used to produce inorganic electrochromic devices (ECDs). This study explores a phenomenon observed in the ferroelectric ε-WO_3 polymorph, which we have named ferroelectric chromism. Evidence presented here supports the claim that the ferroelectric nature of ε-WO_3 plays a key role in the color change observed upon the application of the electric potential to this material. A mechanism for the observed ferroelectric color changing effect is provided in this study as elucidated by X-ray photoelectron spectroscopy analysis. As coloration appears in a single solid-state layer of ε-WO_3 by this chromic effect, developing the next generation of ECDs is possible using this ferroelectric polymorph of WO_3.



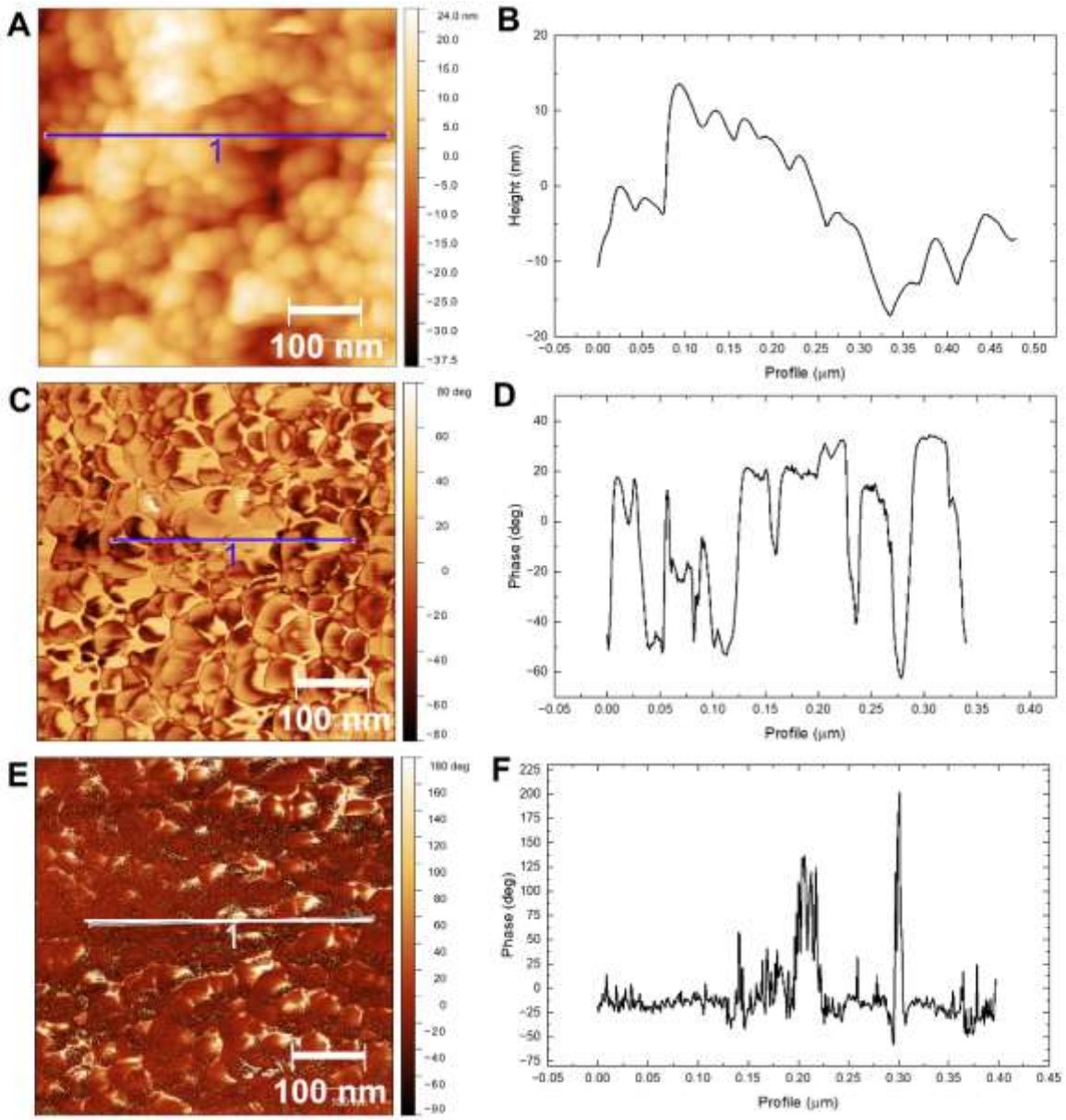


Figure 2. Surface topography and ferroelectric nanodomains of ε−WO_3. (**A, B**) Surface morphology of ε−WO_3 film and height profile measured by AFM. (**C, D**) Out of plane ferroelectric nanodomains of ε−WO_3 and their phase profile. (**E, F**) In-plane ferroelectric nanodomains of ε−WO_3 and their phase profile. [this study is performed at RT using ε−WO_3 film deposited on ITO substrate].

M. M. Rahaman, "Processing and Characterization of Binary Metal Oxide Ferroelectrics", PhD thesis, OSU, Nov 2025.

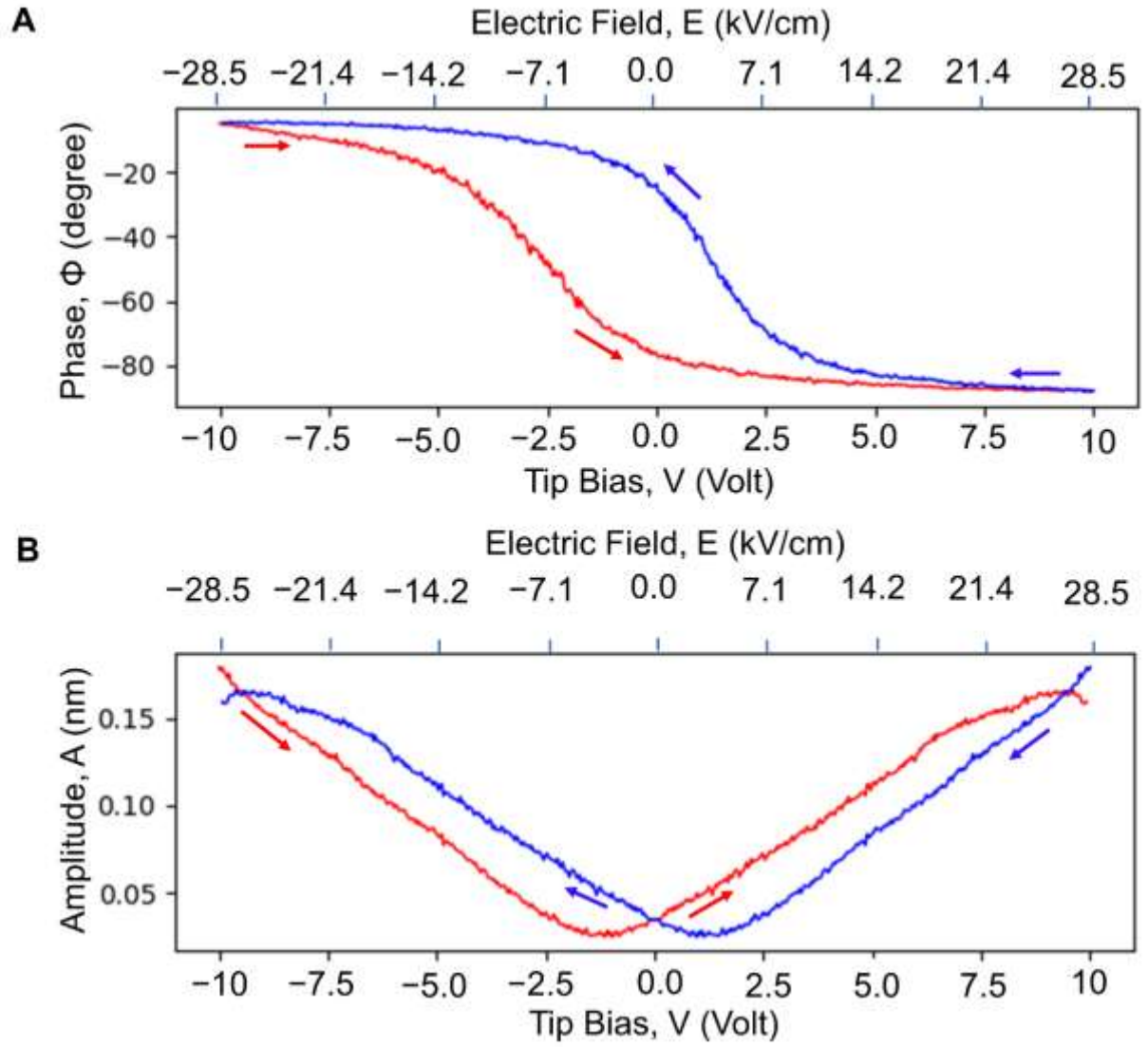
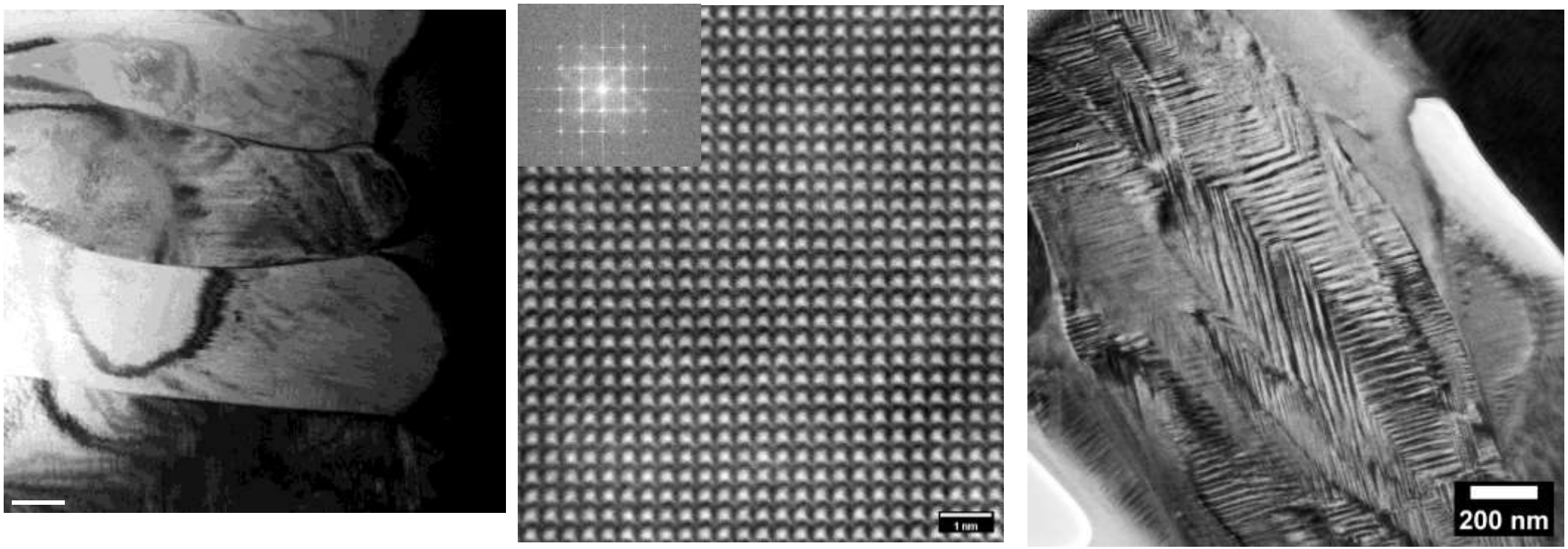


Figure 3. Ferroelectric hysteresis of ε−WO_3 at room temperature. (**A**) Phase switching of the nanodomains of ε−WO_3. and (**B**) Butterfly type hysteresis of amplitude variation of the nanodomains, within ±28.5 kV/cm electric field studied by PFM.

M. M. Rahaman, “Processing and Characterization of Binary Metal Oxide Ferroelectrics”, PhD thesis, OSU, Nov 2025.

Solvothermal synthesis and laser irradiation for the scalable processing of metastable polymorphs

Ceramics International, 50(17), Part B, 31267-31277, 2024

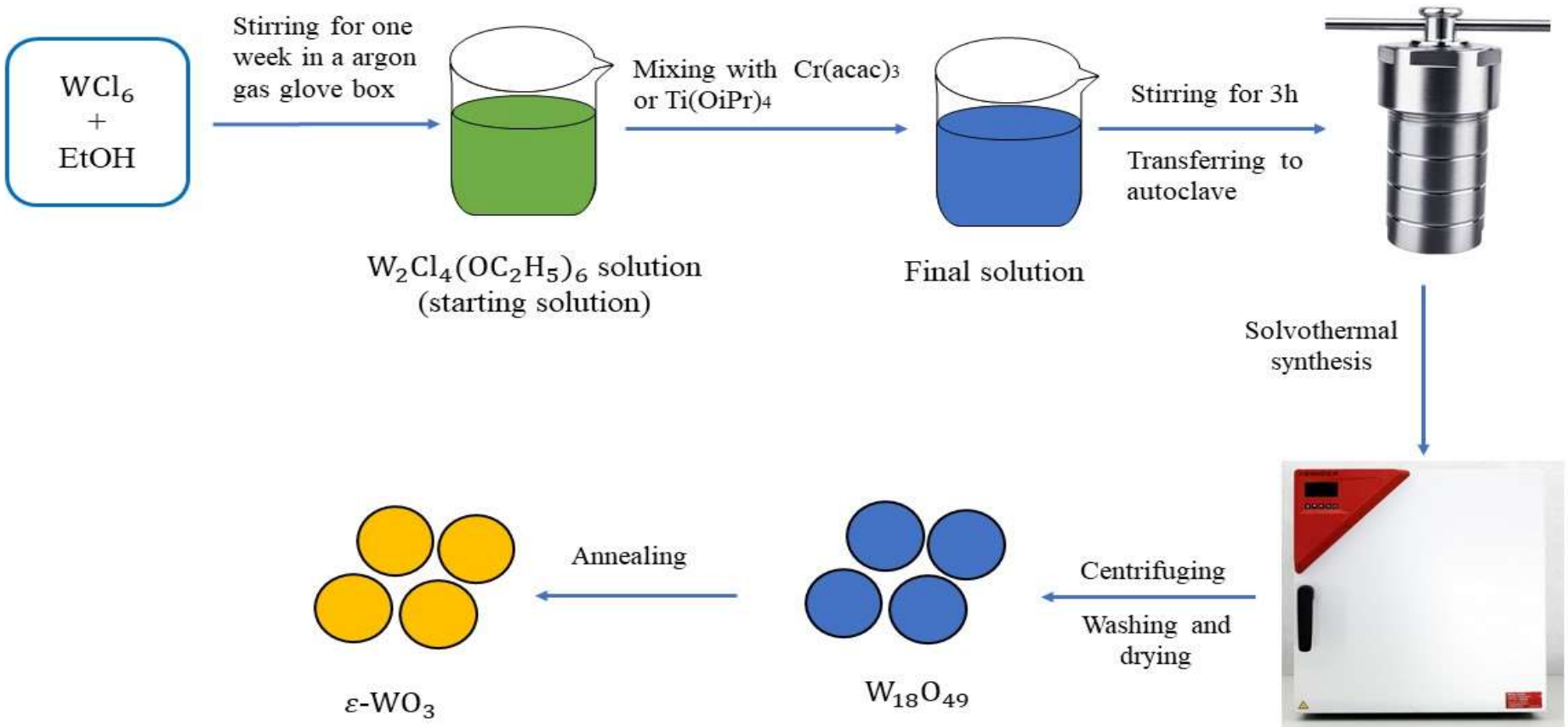


We envision novel laser-based 3D printing of polymorphic materials for in-situ, tailored phase selection

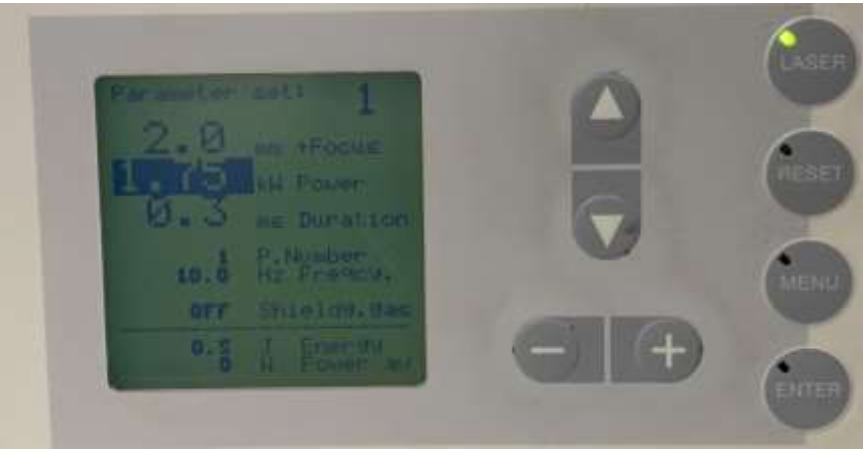
Stabilizing metastable ferroelectric tungsten trioxide phase at room temperature via solvothermal synthesis and millisecond pulsed laser irradiation

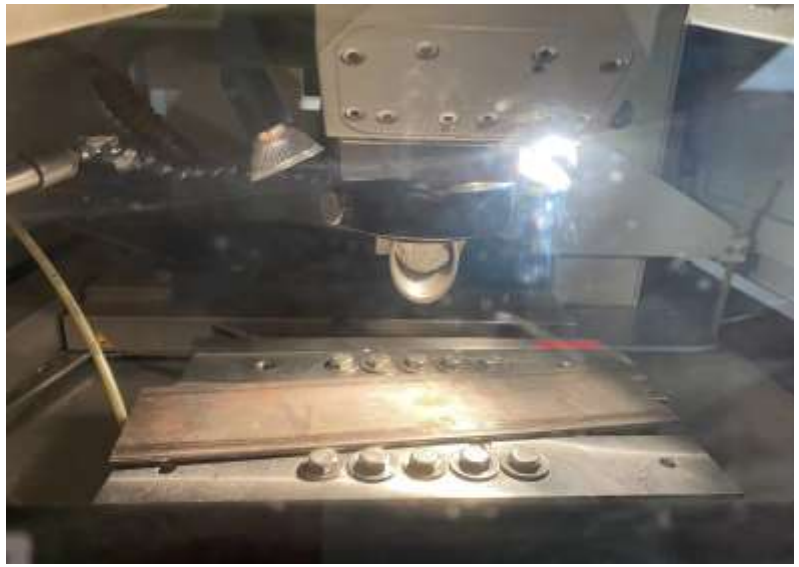
Zanlin Qiu [a,*], Mohammad Mahafuzur Rahaman [a], Boyd Panton [a], Joerg R. Jinschek [b], Pelagia-Irene (Perena) Gouma [a]

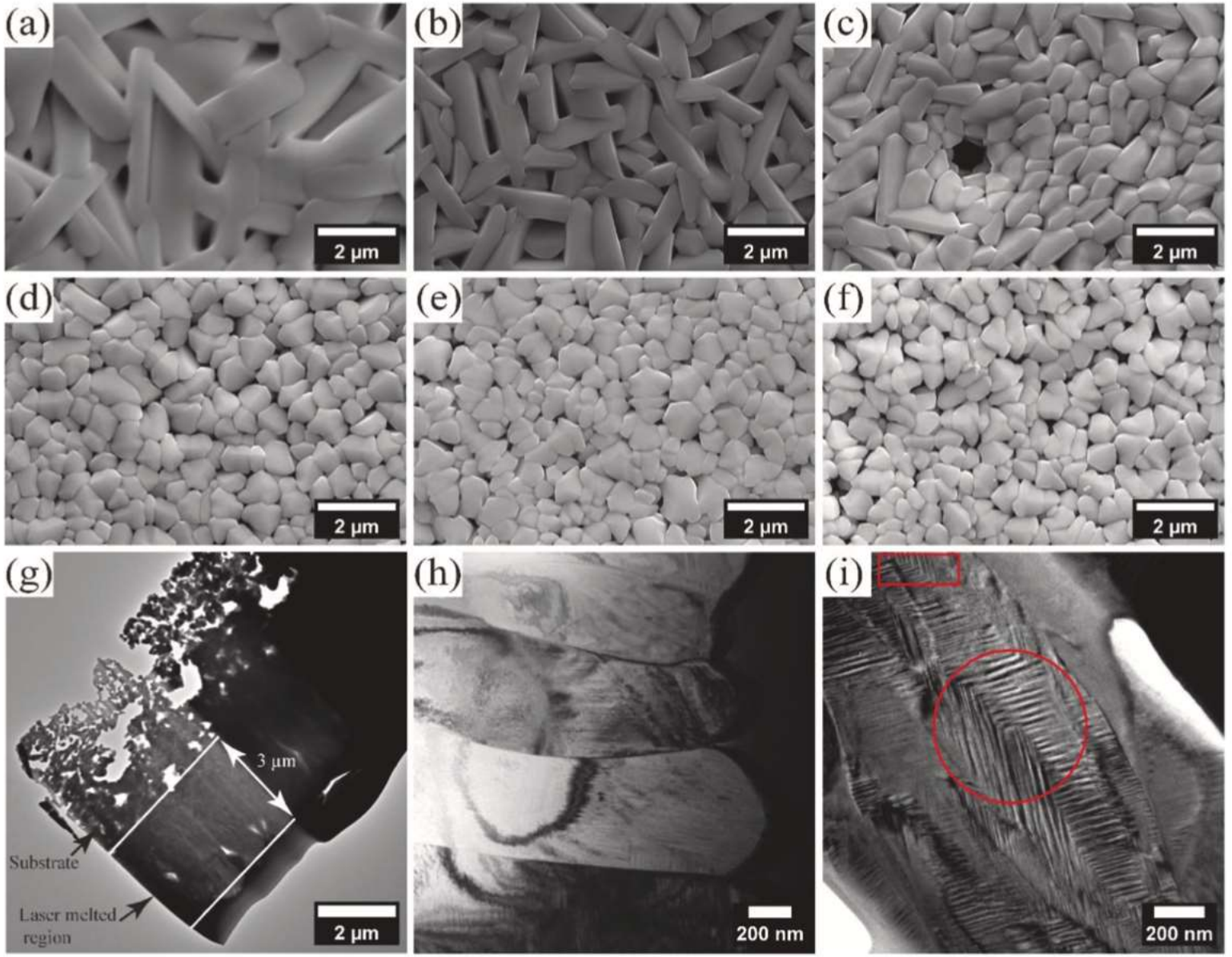
Ceramics International 50 (2024) 31267–31277



Rapid Solidification Processing: Pulse Laser Irradiation







After Laser Irradiation: Almost 100% Conversion to Epsilon

International Journal of Ceramic Engineering & Science

PERSPECTIVE ARTICLE | Open Access

Future insights on high temperature ceramics and composites for extreme environments

Anthony Annerino, Mark Lawson, Pelagia-Irene Gouma

First published: 28 July 2022 | https://doi.org/10.1002/ces2.10156 | VIEW METRICS

SECTIONS PDF TOOLS SHARE

Abstract

This document summarizes key research directions as they emerged during the proceedings of the Inaugural Orton Workshop that aimed to define scientific areas of current interest to the ceramics community around the theme of: *"High Temperature Ceramics and Composites for Extreme Environments."* The topic was selected due to the timely interest in such materials to meet the needs of hypersonic aviation and space exploration and habitation. Experts from funding agencies supporting ceramics research, thought-leaders from academia with expertise spanning materials processing, characterization, and modeling, as well as research and development leaders from key (aviation-related) industries, gathered to evaluate the state-of-the-art in this field and to address key questions with the intent of accelerating research and development efforts on all fronts. Highlights of the work presented and of the discussion and brainstorming sessions are provided here. It was the purpose of the organizers (The Orton Ceramic Foundation and the Orton Chair in Ceramic Engineering at OSU) to establish this event as a service to the Ceramics community in the spirit the founder of the field of Ceramic Engineering, Dr. Edward Orton Jr.

Participant	Affiliation
Thomas Nixon	Rolls-Royce
Todd Steyer	The Boeing Company
Tania Kashyap	Pratt & Whitney
Jim Steibel	GE Aviation
Kara Bridges	Pratt & Whitney
Randall Hay	Wright-Patterson Air Force Base
Lynnette Madsen	National Science Foundation
Frances Hurwitz	National Aeronautics and Space Administration
Jessica Krogstad	University of Illinois Urbana-Champaign
Olivia Graeve	University of California, San Diego
Alexander Mukasyan	University of Notre Dame
David Poerschke	University of Minnesota, Twin Cities
Kathleen Sevener	University of Michigan
Gregory Thompson	University of Alabama
Samantha Daly	University of California, Santa Barbara
Yury Gogotsi	Drexel University
Yunfeng Shi	Rensselaer Polytechnic Institute
Allan Katz	Wright-Paterson Air Force Base
Joseph Homeny	Edward Orton Jr. Ceramic Foundation
Mark Lawson	Edward Orton Jr. Ceramic Foundation
Perena Gouma	The Ohio State University
Garrick Ackart	Edward Orton Jr. Ceramic Foundation
Sheikh Akbar	The Ohio State University
Michael Mills	The Ohio State University
Gregory Morscher	University of Akron

Outlook

Discussions focused on the tremendous task of overcoming industrial aversion to adopting new materials

- <u>Proposed 3-part strategy as solution:</u>
  - Intentionally focusing research on materials with multiple possible applications:
    - For researchers, it increases the chance that their material will be a good fit for an application
    - For industry, a single material for multiple applications simplifies manufacturing concerns
    - Designing a solution in collaboration with others, rather than simply optimizing your one part, is critical
  - Development of evaluation techniques
  - On-going, targeted communication between academic researchers and industry
    - model future academic-industrial collaboration after successful previous government-industry collaborations
    - clearly defined roadmap to industrial adoption with evaluation landmarks along the way that both parties agree on
    - clearly communicated expectations from the start and open communication along the way will seriously accelerate this material maturation process

Industry must drive efforts to develop educated workers for all levels of involvement with these projects from initial research and development to mass production

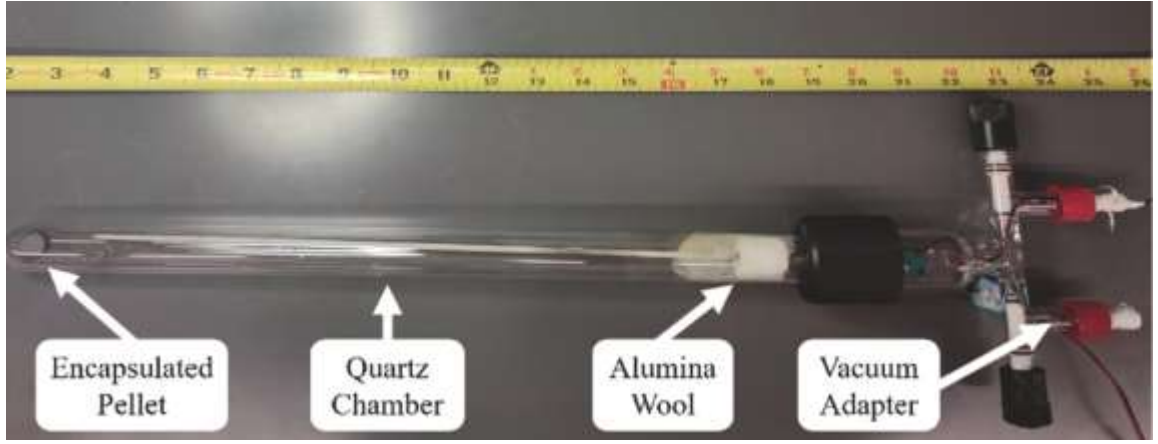
Ceramics International
Volume 50, Issue 22, Part B, 15 November 2024, Pages 47244-47252

SHS of copper Chevrel phase compounds

Tessa Gilmore, Milind Pawar, Perena Gouma

Sample	Mechanism	Flame Wave	Reaction Time
Elemental – 4Cu:6Mo:8S	SDD	Observed	11 s
Layered – 2Cu:4Mo:2MoS_2	Intercalation	Not observed	10 min
Layered – 4Cu:4Mo:2MoS_2	Intercalation	Not observed	10 min
Mixed – 2Cu:4Mo:2MoS_2	Intercalation	Not observed	10 min
Mixed – 4Cu:4Mo:2MoS_2	Intercalation	Not observed	10 min







Video showing SHS process in Chevrel Phase Synthesis from Elemental Precursors-

Note the exothermic reaction propagating and consuming the whole pellet

Received: 10 February 2022 | Revised: 20 July 2022 | Accepted: 25 July 2022

DOI: 10.1111/jace.18724

Journal of the American Ceramic Society

RESEARCH ARTICLE

Intercalation-assisted massive phase transformation: The key to SHS synthesis?

Milind Pawar[1] | **Pelagia-Irene Gouma**[1,2]

[1]Department of Materials Science and Engineering, The Ohio State University, Columbus, Ohio, USA

[2]Department of Mechanical and Aerospace Engineering, The Ohio State University, Columbus, Ohio, USA

Correspondence
Pelagia-Irene Gouma, Department of Materials Science and Engineering, The Ohio State University, Columbus, OH 43210, USA.
Email: gouma.2@osu.edu

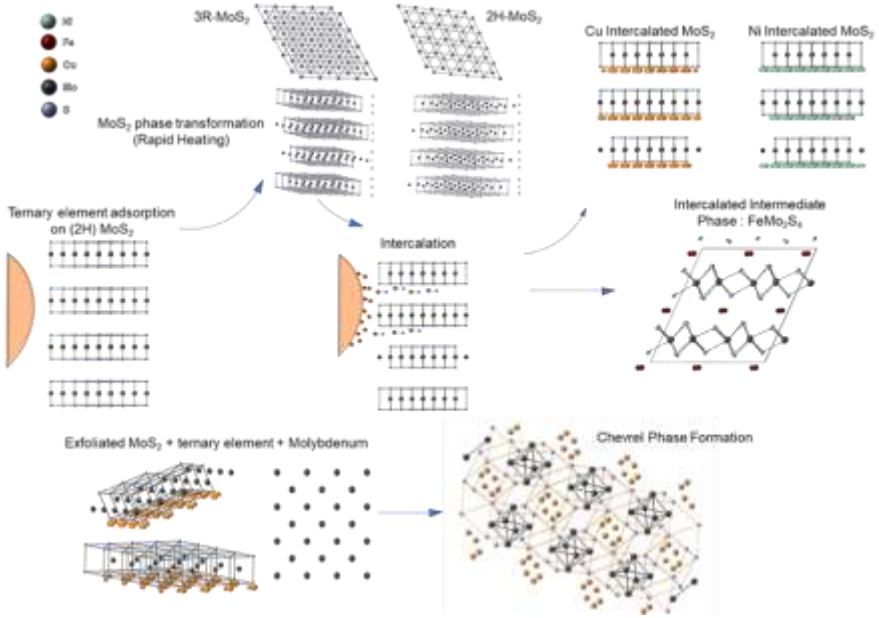
Abstract

Self-propagating high-temperature synthesis (SHS) is the term used for a spontaneous, irreversible combustion of initial reagents when ignited. There is limited knowledge of the mechanistics of this versatile materials synthesis process for Chevrel phase compounds (CPCs), which limits its applicability. In this report, the successful and rapid processing of three classes of sulfide CPCs via SHS is demonstrated, and a mechanism is provided to explain rapid transformation rates and nanostructured products that are fully transformed. $Cu_4Mo_6S_8$, $Ni_2Mo_6S_8$, and $Fe_2Mo_6S_8$ compounds were synthesized, and thermochemical measurements revealed that an overall reaction temperature did not surpass the melting points of the reactants. The nature of the specific SHS process is argued here to involve an intercalation-assisted massive phase transformation facilitated by the use of an MoS_2 precursor.

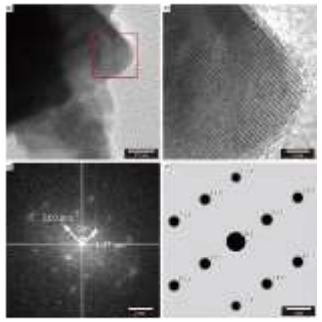
KEYWORDS
scanning electron microscopy, self-propagating high-temperature synthesis, sulfides

CP-Candidate materials for use in critical elements capture

Orton Ceramic Foundation



Triclinic FeMo3S4 (Space group $P\bar{1}$) in [110] *zone axis*



Proposed Reaction Mechanism for the observed rapid and sustainable processing of 2D and 3D ternary chalcogenides

Chevrel Phase Nanofibers

Precursor Solution: N, N dimethylformamide with 5 wt.% PAN

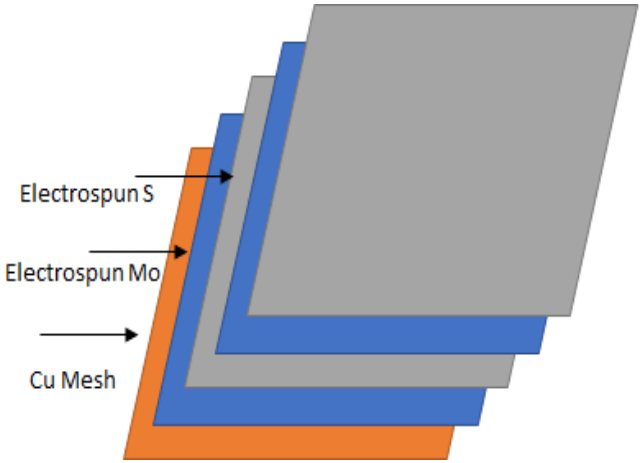
↓

0.01 M Copper (II) Chloride, 0.03 M Molybdenum (V) Chloride, 0.04 M Thiourea

↓

Electrospinning: Volume 10 ml, Working distance 8 cm, Flow rate 0.5 ml/ hr, Applied voltage 10 kV

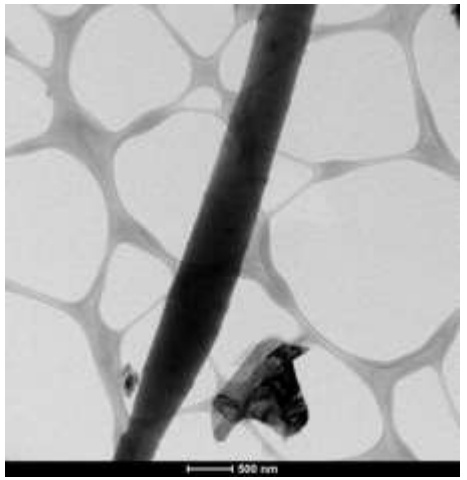




SHS for as-spun fibers







Unpublished research, OSU, 2022-2026

Overview

- **The Advanced Materials Research Lab has been processing ceramic and composite materials with diverse functionality**
- **Polymorphic Oxides, WO_3, MoO_3, HfO_2, TiO_2 , Y_2O_3, Al_2O_3, etc. have been processed by various methods (including electrospinning) and can be found as single crystal nanowires and as 3D woven or non-woven fibrous mats for reinforcements**
- **We have developed a modified SHS process which allows for temperature-controlled processing of any type of material from layered intercalation compounds**
- **Combining contemporary ceramic synthesis with laser post-processing we can maintain metastable phases and unique functionality**
- **Whether for functional or for structural applications, we have demonstrated oxides and sulfides made from energy efficient, scalable, and cost-effective processes**

Sponsors



Addendum: Sensor Materials and Technologies

Breath Gases as Disease Markers

Biomarkers in exhaled breath

Human breath is a very complex mixture of chemical compositions

The majority part of our exhaled gases consists of nitrogen, oxygen, carbon dioxide, water and inert gases

The remaining small fraction of breath contains thousands of components in trace amount, including inorganic gas molecules like nitric monoxide and diverse kinds of volatile organic compounds (VOCs)

Biomarkers	Physiological origin	Related diseases	Physiological ranges in human breath
Ethane	Lipid peroxidation	Oxidative stress	1-11 ppb
Pentane	Lipid peroxidation	Oxidative stress	Less than ethane
Isoprene	Cholesterol biosynthesis	Cholesterol metabolic disorder	55-121 ppb; 12-580 ppb;
Acetone	Decarboxylation of acetoacetate and acetyl-CoA	Diabetes mellitus, ketonemia	293-870 ppb; 1.2-1880 ppb
Ethanol	Alcohol ingestion	Alcohol poisoning	27-153 ppb; 13-1000 ppb
Methanol	Degradation of natural pectin from plants; ingestion	Methanol intoxication	160-2000 ppb
NH_3	Metabolic product of amino acid deamination	Uremia, kidney impairment	422-2389 ppb; 200-1750 ppb
CO	Inhalation from Incomplete burning of carbon containing fuels, e.g. smoking	Lung diseases	<6 ppm
NO	L-arginine oxidation	Asthma, lung diseases	1-9 ppb, lower respiratory; 0.2-1 ppm upper respiratory; 1-30 ppm, nasal level.

A. Amann and D. Smith, *Breath Analysis for Clinical Diagnosis and Therapeutic Monitoring,* World Scientific, Singapore, 2005

Artificial Olfaction-Selective Gas Sensors

P. Gouma, *Science of Advanced Materials*, 3(5), pp. 787-793, 2011.

Material Science approach

- **Disruptive sensing technology**
- **Personalized medicine tools**
- Rely on **selective chemosensing**
- they detect specific biomarkers in exhaled breath

CRYSTALLO-CHEMICAL APPROACH TO SELECTIVE CHEMOSENSING



Group A: oxides having the ReO_3 structure

(γ-WO_3, β-MoO_3)

NO

marker for inflammation in lungs

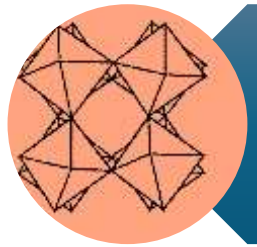


Group B: oxides having a weakly bonded layered structure

(α-MoO_3, h-WO_3)

Ammonia

marker for renal diseases



Group C: acentric crystal structures-ferroelectric polymorphs

(ε-WO_3)

Acetone

correlates with insulin levels in the body



Group D: oxides having the rutile structure

(TiO_2, SnO_2, IrO_2, MnO_2)

CO

marker for cardiovascular diseases

Our unique COVID-19 Breath Test, 2020

A Covid Test as Easy as Breathing

Scientists have been dreaming of disease-detecting breathalyzers for years. Has the time for the technology finally come?

Give this article



Sarah Karow, a clinical research coordinator at Ohio State University, demonstrated a prototype breathalyzer, under F.D.A. review, that is designed to detect Covid-19. Maddie McGarvey for The New York Times

Lessons learned from Our COVID-19 Breath Test

- We used a symptomatic population (patients coming through the ER) to establish the breath-print for this disease-*ICU study* (published)

- We were also able to identify a sensitivity index in the olfactory pattern which was an indicator of the improvement of the patient status until fully recovered

- We also carried out *Ambulatory studies* which confirmed the accuracy of the breath-print for COVID-19

- There is also a very distinct breath pattern for the control group which was not exposed to any infectious diseases

OPEN ACCESS PEER-REVIEWED

RESEARCH ARTICLE

Exhaled nitric oxide detection for diagnosis of COVID-19 in critically ill patients

Matthew C. Exline, Milutin Stanacevic, Andrew S. Bowman, Pelagia-Irene Gouma

Published: October 28, 2021 • https://doi.org/10.1371/journal.pone.0257644

38 Save | 17 Citation | 7,517 View | 39 Share

Abstract
Introduction
Methods
Results
Discussion
Supporting information
Acknowledgments

Abstract

Background

COVID-19 may present with a variety of clinical syndromes, however, the upper airway and the lower respiratory tract are the principle sites of infection. Previous work on respiratory viral infections demonstrated that airway inflammation results in the release of volatile organic compounds as well as nitric oxide. The detection of these gases from patients' exhaled breath offers a novel potential diagnostic target for COVID-19 that would offer real-time screening of patients for COVID-19 infection.

Download PDF | Print | Share

Check for updates

Included in the Following Collection

COVID-19 pandemic (2019-21)

ADVERTISEMENT

DIU/DTRA project funded in 2023

Mitigating the spread of respiratory illnesses: DOD funds research into portable, easy-to-use breath analyzers



[Image above] A new program housed under the U.S. Department of Defense aims to accelerate development of breath analyzers for rapid diagnosis of respiratory illnesses among warfighters. Credit: Jose Rodriguez (Army), U.S. Department of Defense

In August 2023, Gouma's expertise in breath analysis was recognized when her group at OSU was the third organization to receive funding under the U.S. Department of Defense's new EXHALE Program.

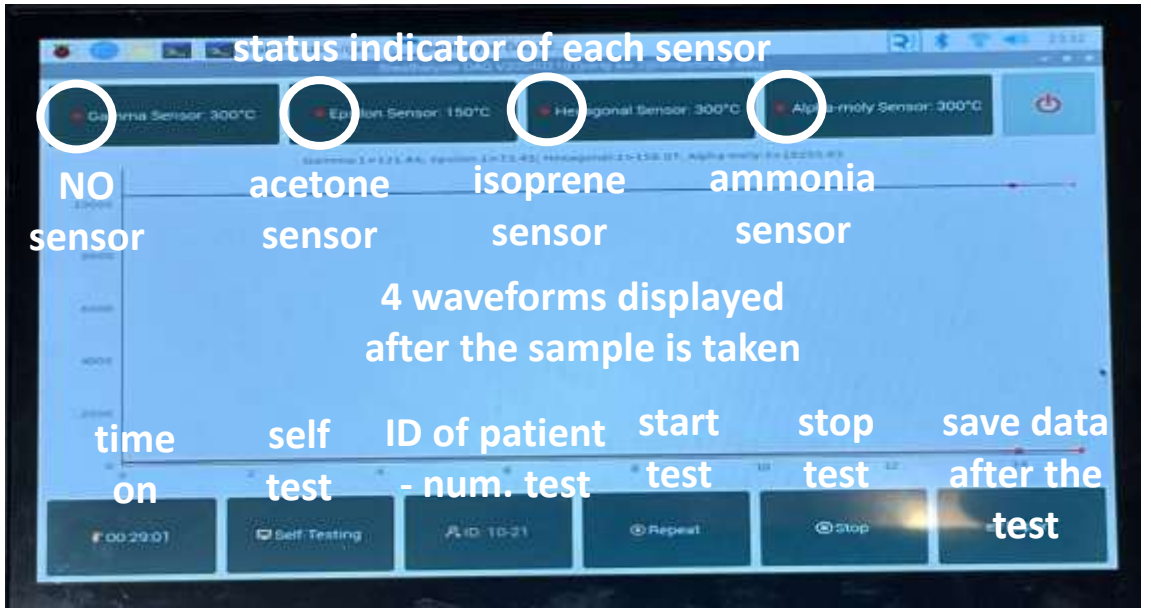
The EXHALE Program is a partnership between the Defense Department's Defense Threat Reduction Agency and Defense Innovation Unit. Launched in May 2023, it aims to accelerate development of portable, easy-to-use breath analyzers for rapid diagnosis of respiratory illnesses among warfighters.

The prototype breath analyzers developed through the EXHALE Program will be acquired by the Defense Department through an Other Transaction Authority (OTA) agreement. OTAs have been a feature of the government acquisition system for decades, but it is only recently that the Defense Department started making heavy use of this acquisition mechanism.

Prototype 1G



Prototype 1G delivered to OSU WMC for clinical testing



Prototype 1G graphical user interface (GUI)

- The sample is collected with a single exhale from the subject
- The recorded signal presents the resistance of the sensor, which is proportional to a specific analyte concentration over the sensor
- The resistance waveform for each of the four sensors is converted to digital domain
- The samples are recorded for 30 seconds, and the clinical coordinators are instructed to ask subject to start exhale around 5 seconds after the recording starts

Test: COVID vs Control Group

	Positive	Negative	
Pos	12	6	18
Neg	5	30	35
	17	36	

Sensitivity	71%
Specificity	83%
PPV	67%
NPV	86%
Accuracy	79%

Test design:

6 patients have a distinct reverse omega pattern in NO sensor

S_{end} values in acetone and ammonia sensor (positive is high in acetone and low in ammonia)

S and S_{end} in isoprene sensor (positive is high in isoprene)

Test: Parainfluenza vs Control Group

For the test in the parainfluenza group against the patients in the control group, we use the S and S_{end} values in acetone sensor

	Positive	Negative	
Pos	5	4	9
Neg	3	32	35
	8	36	

Sensitivity	63%
Specificity	89%
PPV	56%
NPV	91%
Accuracy	84%

Test design:

High S values in acetone and low value in S_{end}

observing the parainfluenza group against the patients in the control group